Interaction of Mechanical Systems with Structurally Significant Fire Events and Tunnel Fire Mitigation Optimization

FINAL PROJECT REPORT

by
Zheda Zhu
Spencer Quiel
Clay Naito

Lehigh University

Sponsorship
(List UTC-UTI and cost matching external sponsors)

For

University Transportation Center for
Underground Transportation Infrastructure
(UTC-UTI)

September 30, 2022

Disclaimer

The contents of this report reflect the views of the authors, who are responsible for the facts and the accuracy of the information presented herein. This document is disseminated in the interest of information exchange. The report is funded, partially or entirely, by a grant from the U.S. Department of Transportation's University Transportation Centers Program. However, the U.S. Government assumes no liability for the contents or use thereof.

1. Report No.	2. Government Accession No.	3. Recipient's Catalog No.	
4. Title and Subtitle: Interaction of Mechanical Systems with Structurally Significant Fire Events and Tunnel Fire Mitigation Optimization		5. Report Date 09/30/2022	
		6. Performing Organization Code	
7. Author(s) Zheda Zhu, Ph.D.; Spencer Quiel, Ph.D.; Clay Naito, PhD		8.Performing Organization Report No.	
9. Performing Organization Name and Address University Transportation Center for Underground Transportation Infrastructure (UTC-UTI) Tier 1 University Transportation Center Colorado School of Mines Coolbaugh 308, 1012 14th St., Golden, CO 80401		10. Work Unit No. (TRAIS)	
		11. Contract or Grant No.	
12. Sponsoring Agency Name and Address United States of America Department of Transportation Research and Innovative Technology Administration		13. Type of Report and Period Covered	
		14. Sponsoring Agency Code	
15. Supplementary Notes Report also available at: https://zenodo.org/communities/utc-uti			
16. Abstract The first section of this report numerically investigates the thermal impact of vehicle fire hazards on exposed electrical conduits in roadway tunnels. By modeling the fire and subsequent heat transfer to the conduit, the analysis results provide performance-based design guidance for allowable temperature increases before the conduit and its contents fail. The computationally efficient Confined Discretized Solid Flame (CDSF) model (previously developed by the authors) is used to calculate the heat flux imparted to the tunnel conduit from the enclosed fire. A simplified finite element model is used to calculate the subsequent thermal response of the conduit piping. Envelopes of conduit temperature increase, as well as exposure duration, are developed for a range of vehicle fire intensities that are enclosed in two- and three-lane circular tunnels. By accounting for overall traffic volume and truck traffic percentage, the limiting criteria for conduit temperature increase during standard experimental testing can be associated with a return period or a probability of exceeding an expected temperature. The second section outlines a new decision-making approach to optimize fire mitigation strategies for roadway tunnels by minimizing the initial investment and life cycle costs and maximizing the protection efficiency. First, a concrete liner damage assessment tool is developed that accounts for the use or non-use of passive fire protection and the realistic uncertainties in the thermal properties of the materials used. Second, the investment, as well as the economic loss due to stochastic vehicle fire hazards, are quantified for a single mitigation strategy or a combination of strategies. The economic loss includes the direct repair cost and the functionality loss due to tunnel closure, which is determined by the extent and severity of concrete liner damage and the corresponding repair procedures. Third, a genetic algorithm is used to perform a multi-objective optimization, resulting in a Pareto front as the reference for the decision-making process.			
17. Key Words: conduit; CDSF model; mitigation; optimization; tunnel; fire		18. Distribution Statement No restrictions.	
19. Security Classification (of this report) Unclassified	20. Security Classification (of this page) Unclassified	21. No of Pages 81	22. Price NA

Table of Contents

Table of Contents 4
List of Figures 6
List of Tables 8
EXCUTIVE SUMMARY 10
CHAPTER 1 – PERFORMANCE-BASED EVALUATION OF EXPOSED ELECTRICAL CONDUIT FOR SEVERE FIRES IN ROADWAY TUNNELS 13
1.1. Introduction 13
1.2. Existing fire resistance 15
1.3. Performance-based approach 16
1.3.1. CDSF modeling of the fire and heat transfer 16
1.3.2. Design fire time history 21
1.3.3. FE thermal analysis of the conduit 23
1.3.4. Correlating heat flux exposure to internal conduit temperature 25
1.4. Parametric study for internal conduit temperature 26
1.4.1. Analysis matrix 27
1.4.2. Conduit location and exposure percentage 28
1.5. Thermal threshold selection based on tunnel traffic 31
1.5.1. Sensitivity study 35
1.6. Conclusions 37
CHAPTER 2 – PERFORMANCE-BASED OPTIMIZATION OF STRUCTURAL FIRE MITIGATION STRATEGIES FOR ROADWAY TUNNELS 39
2.1 Introduction 39
2.2 Framework and methodology 40
2.2.1. Damage assessment for the concrete liner with passive fire protection 41
2.2.2. Protection Investment 52
2.2.3. Tunnel fire impact calculation through CDSF model 55
2.2.4. Economic loss due to fire hazard 56
2.2.5. Mitigation optimization 62
2.3. Case study 63
2.3.1. Prototype tunnel 63
2.3.2. Optimization problem set up 64
2.3.3. Results and discussion 65
2.4. Sensitivity analysis 68

2.4.1. Influence of tunnel dimension 68
2.4.2. Influence of traffic 69
2.4.3. Influence of tunnel detour length 70
2.5. Conclusion 72
REFERENCE 74
APPENDIX A – TECHNOLOGY TRANSFER ACTIVITIES 79
1. Accomplishments 79
2. Participants and Collaborating Organizations 80
3. Outputs 81
4. Outcomes 81
5. Impacts 81

List of Figures

Figure 1: CDSF model illustration within a circular tunnel cross-section 19
Figure 2: Illustrative examples of total heat flux from the CDSF model for a 100MW fire within a 2-lane circular tunnel cross-section 21
Figure 3: Total combustion energy for tunnel fires as a function of peak HRR 22
Figure 4: HRR time histories considered for this study 23
Figure 5: SAFIR thermal analysis results for conduit at steady state 24
Figure 6: Average internal surface temperature time history of typical conduit piping for ASTM E1529 heat flux and temperature demands (ASTM International 2016) 25
Figure 7: Relationship between average internal conduit surface temperature and applied heat flux 26
Figure 8: Cross-sectional locations for conduit pipe installation 27
Figure 9: Maximum thermal load on the conduit at the top of the tunnel ceiling 29
Figure 10: Maximum thermal load on the conduit at Sidewall Location 1 per Figure 8 30
Figure 11: Maximum thermal load on the conduit at Sidewall Location 2 per Figure 8 30
Figure 12: Internal conduit temperature at the top of the tunnel ceiling for varying exposure percentage 31
Figure 13: Cumulative probability of tunnel fire intensity in terms of HRR 34
Figure 14: Maximum internal conduit temperature thresholds based on fire hazard and traffic data 35
Figure 15: Influence of AADT and tunnel length on maximum internal conduit temperature 36
Figure 16: Influence of HGV traffic percentage on maximum internal conduit temperature 37
Figure 17: Flowchart of tunnel fire protection optimization 41
Figure 18: Thermal properties of the protection board and SFRM 43
Figure 19: Prototype concrete tunnel liner geometry and fiber model 45
Figure 20: Flowchart of thermal analysis and damage classification for concrete liner 47
Figure 21: Damage classification tool for concrete panel with fire protection board of 8mm 49
Figure 22: Damage classification tool for concrete panel with fire protection board of 15mm 49
Figure 23: Damage classification tool for concrete panel with SFRM of 12.7mm (0.5in) 50
Figure 24: Further concrete removal depth of heavy damaged class and surface regression for prediction 52
Figure 25: Distribution of (a) heat flux (b) damage state (c) repairing time and (d) repairing cost for the natural ventilated 3-lane circular tunnel with 8mm fire protection board subjected to fire hazard of 200MW 56
Figure 26: Uncertainties associated with tunnel fire impact 61
Figure 27: Circular tunnel cross-section 64
Figure 28: HRR probability distribution based on tunnel traffic 64

Figure 29: Pareto front generated via genetic algorithm for southbound Lehigh Tunnel 66
Figure 30: Influence of tunnel dimension on optimal fire mitigation 69
Figure 31: Influence of tunnel traffic on optimal fire mitigation 70
Figure 32: Influence of tunnel importance on optimal fire mitigation 71

List of Tables

Table 1: Existing standard testing methods for conduit 16
Table 2: Summary of combustion energy and peak HRR from the results of published fire tests 21
Table 3: Peak HRRs of vehicle fires used for analysis in this study 22
Table 4: Parametric matrix for evaluating conduit response to fire 28
Table 5: Breakdown of tunnel traffic composition, representative combustion weight, and peak fire HRR by vehicle type [44] 33
Table 6: Parametric study of tunnel traffic 36
Table 7: Thermal material of the fire protection board 43
Table 8: Input parameters for protected concrete damage assessment tool development 48
Table 9: Parameters for damage classification boundaries for specific passive fire protection 51
Table 10: Investment for tunnel fire protection methods 54
Table 11: Protected tunnel concrete liner repair procedure post-fire 57
Table 12: Repairing cost for protected tunnel concrete liner 59
Table 13: Parameters for traffic-related economic loss assessment 60
Table 14: Typical 2-lane traffic composition and fire rate 64
Table 15: Optimal fire protection for southbound Lehigh Tunnel 67
Table 16: Optimal solutions influenced by traffic volume 70
Table 17: Optimal solutions for tunnel with various detour lengths 71

List of Abbreviations

CDSF: Confined Discretized Solid Flame

HRR: Heat Release Rate

HGV: Heavy Goods Vehicle

EXCUTIVE SUMMARY

Overview:

The first section of this report investigates the thermal impact of vehicle fire hazards on exposed electrical conduits in roadway tunnels. By modeling the fire and subsequent heat transfer to the conduit, the analysis results provide performance-based design guidance for allowable temperature increases before the conduit and its contents fail. The computationally efficient Confined Discretized Solid Flame (CDSF) model (previously developed by the authors) is used to calculate the heat flux imparted to the tunnel conduit from the enclosed fire. A simplified finite element model is used to calculate the subsequent thermal response of the conduit piping. Envelopes of conduit temperature increase, as well as exposure duration, are developed for a range of vehicle fire intensities that are enclosed in two- and three-lane circular tunnels. By accounting for overall traffic volume and truck traffic percentage, the limiting criteria for conduit temperature increase during standard experimental testing can be associated with a return period or a probability of exceeding an expected temperature. Sensitivity analyses are performed to examine the influence of conduit size and material, conduit location, tunnel ventilation conditions, average annual daily traffic, and traffic composition.

Several technologies such as forced ventilation, active fire-fighting systems, and passive fire protection systems are used in current practice to mitigate fire-induced structural damage and increase resilience for roadway tunnels. Decisions about the cost-benefit of each strategy will be based on a tunnel's geometry, traffic load, and repairability; however, there are few available performance-based tools that account for the comparative impact of each strategy on reducing post-fire downtime and cost. The second section outlines a new decision-making approach to optimize fire mitigation strategies for roadway tunnels by minimizing the initial investment and life cycle costs and maximizing the protection efficiency. This proposed approach is then used to evaluate the sensitivity of fire protection selection to tunnel geometry, traffic volume and composition, and detour length during closure.

Findings:

(1) The confined discretized solid flame (CDSF) model previously developed by the authors can efficiently calculate the incident heat flux on the conduit due to vehicle fires with varying intensities, the range for which is obtained from NFPA 502. Both naturally ventilated and longitudinally ventilated (with airflow at critical velocity) conditions can be considered.

(2) Due to their small thermal mass, the temperature increases in the conduit pipe when subjected to fire is not sensitive to its steel material type or sizing. However, the conduit temperature is significantly affected by the percentage of surface area that is exposed to heating. A conservative correlation is developed

to calculate the internal conduit temperature as a function of the incident heat flux and surface area exposure percentage.

(3) The peak total heat flux imparted by the fully developed fire at every tunnel location is associated with a time history per Ingason's quadratic design curve for tunnel fires [33]. The sensitivity of the curve parameters to total fuel load, growth rate, and decay rate were examined. For all vehicle fire scenarios considered in this study, the total duration of thermal exposure does not exceed 2.5 hours. Based on the results, the peak thermal exposure duration for a standard test to determine conduit fire resistance could range from 30 minutes to 2 hours, depending on a user-defined threshold of fire hazard severity.

(4) Based on the results of parametric analyses, the thermal impact on exposed electrical conduit can be quantifiably reduced by (1) implementing longitudinal ventilation at critical velocity, (2) reducing the exposure surface area, and (3) relocating the installed location from the ceiling to the sidewall.

(5) The proposed performance-based approach can enable the selection of tunnel conduit thermal performance criteria as a function of tunnel geometry, ventilation conditions, conduit configuration, and tunnel traffic composition. Due to the importance of continued operation of a tunnel's electrical systems during an emergency, the thermal performance rating for these conduits can be determined as risk tolerance based on expected fire intensity rather than via simple prescriptive thresholds.

(6) For the conduit considered in this study, performance-based evaluation based on traffic data provided by PennDOT indicated that the following exposure thresholds could be used to develop risk-based fire resistance ratings for conduits that run along the circular tunnel's top-of-ceiling and are fully exposed to fire:

- To withstand a 50-yr return period fire, the conduit and its contents should remain functional after 2 hrs of exposure to 1095°C (consistent with the mean prescribed value in ASTM E1529) if the tunnel has longitudinal ventilation at critical velocity. Similarly, an exposure temperature of 1500°C would apply for natural ventilation conditions.
- For a 20-yr return period fire, the corresponding temperature demands decrease to 1150°C and 900°C for the natural and longitudinally ventilated cases, respectively.

(7) The MATLAB-SAFIR method is efficient to model the behavior of the concrete liner protected with passive fire protection subjected to fire hazards. Considering the uncertainties associated with the thermal parameters of both concrete liner and protection materials with MCS, the damage maps are developed to help efficiently characterize the damage state of the protected concrete liner.

(8) With the computational efficiency of the confined discretized solid flame (CDSF) model and damage maps developed in this study, the entire tunnel damage along with the repairing time and cost afterward, can be assessed as subjected to specific tunnel fire hazard.

(9) The lifecycle investment for a specific fire protection plan is calculated, containing the installation and maintenance fee, while the lifecycle loss due to the tunnel fire hazard is assessed based on the tunnel traffic and its importance. The uncertainties associated are considered via MCS taking the 95% confidence interval.

(10) The multi-objective optimization via GAs provides optimal solutions while contradictory objectives are applied. This optimization method is flexible in choosing the objectives and constraints as needed according to specific engineering requirements. Carefully choosing the appropriate objective sets can help narrow down decision-making choices.

(11) The factors influencing the optimal solutions include the tunnel traffic and the detour length. Generally, tunnel of smaller size, higher traffic volume, higher HGV percentage, longer detour length requires more protection. The longitudinal ventilation, though required for life safety concerns, is not efficient for mitigating the tunnel structural damage compared to the FFFS and protection boards.

CHAPTER 1 – PERFORMANCE-BASED EVALUATION OF EXPOSED ELECTRICAL CONDUIT FOR SEVERE FIRES IN ROADWAY TUNNELS

1.1. Introduction

When in operation, roadway tunnels are continually at risk of experiencing damage from vehicle fire hazards. The thermal demands generated from a fully developed fire in a tunnel can cause significant damage to both structural and nonstructural elements of the tunnel system, depending on the fire intensity and duration. The fire-induced response and damage pertaining to the tunnel structure have received significant engineering and research attention in numerous recent studies (Bergmeister et al. 2020; Gehandler 2015; Guo et al. 2020a; Hua et al. 2021; Ouyang et al. 2021; Pichler et al. 2006; Sýkora et al. 2018). In this regard, thermal impact from the fire can range from localized structural damage (Pichler et al. 2006; Schrefler et al. 2002) up to progressive collapse (NFPA 2017 p. 502) of the tunnel liner, and partitioning structures such as drop ceiling panels (Ouyang et al. 2021) can also be adversely affected.

Compared to the tunnel structure, there is much less research literature on the fire resistance of important nonstructural components that are vital to the operation of the tunnel both during and after a fire event, including electrical conduits, jet fans, lighting systems, and fixed firefighting systems (FFFS) (USDOT 2015). For example, a study by the Permanent International Association of Road Congresses (PIARC) emphasized the importance of fire resistant design for the components that comprise a tunnel ventilation, so that it is not easily impaired by a fire event (PIARC 2007). Per PIARC, equipment units such as the ventilation fans themselves are typically protected with insulation and can remain functional when exposed to 250°C for 1-2 hrs, while fire resistant cables should be able to withstand 950°C for up to 3 hours (PIARC 2022). For building applications, vendor guidelines are available (OBO Betterman 2019) for choosing the appropriate conduit types to limit smoke generation and toxic gas as well as fire spread. Protection materials are recommended along with fire resistant attachment techniques to maintain operation and to protect occupants during an event. Holland et al. (Holland et al. 2015) experimentally studied the effects of compartment fires on electrical cable supports up to 600°C and found that the cable system can remain intact as long as the mechanical attachment is capable of surviving the fire event. In tunnel applications, electrical conduit is typically installed on the surface of the tunnel liner (along either the ceiling or sidewall) and will be exposed to enclosed vehicle fires unless protected with passive fire protection or placed behind nonstructural paneling. While fire protection of these components is an obvious objective toward maintaining tunnel operability during and after a fire event, there remains a need for clear performance metrics when subjected to a range of heat intensities and durations.

This study investigates the performance of standard steel conduit piping when exposed to vehicular fire effects in roadway tunnels. The existing criteria for tunnel conduit fire safety rely on uniform temperature benchmarks that are assumed to be applied over a specified time duration (ASTM International 2016, 2019; National Fire Protection Association 2007; UL Standard 2017). For example, UL Standard 2196 (UL Standard 2017) requires wires within the electrical conduit to maintain a signal connection after exposure to 1000°C (1850°F) for 2 hours. Though conservative in most cases, these criteria do not necessarily correlate to expected thermal impacts from realistic tunnel fire hazards. As an example, the thermal demands from a heavy goods vehicle (HGV) fire event can exceed the UL 2196 prescribed temperature limits (Ingason et al. 2011). In addition, due to a limited supply of combustible fuel in most vehicle-based tunnel fire events, burn-out of a fully developed fire can occur in less than two hours; however, high temperatures at a level lower than the UL 2196 threshold may persist for longer than two hours in the enclosed, concrete-lined environment.

The performance-based approach presented in this paper will demonstrate that the thermal response criteria can be tailored to account for variability in the vehicle fire intensity and duration; the electrical conduit sizing, material, and installed location; and the roadway tunnel's geometry, ventilation conditions, and traffic conditions. The thermal impact on tunnel conduit from a vehicle fire can be evaluated using either computational fluid dynamics (CFD) modeling approaches (Li et al. 2017; McGrattan et al. 2013) (in which the enclosed fire and the heat transfer to the conduit are modeled via high fidelity numerical simulations) or through semi-empirical methods developed based on a combination of first principles and test data. CFD simulations can provide a detailed prediction of thermal effects in terms of heat flux and temperature (which can be used as the thermal load on the conduit) and can be tailored to a wide range of tunnel geometries, ventilation layouts, and fire scenarios. CFD simulations also require deep understandings of the numerical inputs associated with the fire properties, heat transfer modes, discretization layouts, and airflow transfer, which can all affect the simulation results to varying degrees. Validation and discretization sensitivity studies are needed to ensure that the CFD modeling approach is applied appropriately for a given application. Moreover, CFD approaches are also computationally expensive, which may limit their use when examining a large number of research variables or fire scenarios.

By contrast, semi-empirical methods can consider the characteristics of generic tunnels and fire hazards with a much smaller array of input variables than CFD models, and they are significantly more computational efficient for parametric evaluation of thermal loads. The semi-empirical Confined Discretized Solid Flame (CDSF) model has been developed previously by the authors to evaluate the thermal impact of large fires on the exposed inner surfaces in both natural (Guo et al. 2019) and longitudinally ventilated (Zhu et al. 2022) tunnels. The CDSF model considers the total thermal impact from both flame+smoke radiation (calculated as emission from a 3D solid flame object) and convective

from the combustion byproducts (calculated using a data-driven correlation between fire intensity and tunnel geometry). As a non-iterative method, the CDSF model is well-suited for parametric evaluation of that account for uncertainties associated with both fire and tunnel conditions. In previous work, the CDSF model has shown strong agreement with both experimental test results and high-fidelity numerical simulations conducted using the Fire Dynamic Simulator (FDS) (Guo et al. 2019; Zhu et al. 2022). The model can be adapted to tunnels of different shapes and dimensions, and it can accommodate peak fire intensities from 5-300 MW with either natural ventilation or longitudinally ventilated conditions.

This study combines the CDSF model with thermal finite element analyses to calculate the thermal impact of severe vehicle fire scenarios on typical tunnel electrical conduit piping. Temperature exposure intensities and fire exposure lengths are proposed as a means of performance-based design to resist realistic tunnel fire hazards, and these metrics can be used to shape the approach for fire resistance testing. Several sensitivity analyses are conducted to examine the influence of conduit material and sizing on the resulting thermal response. Tunnel traffic volume and composition (particularly truck traffic) are used to provide a probabilistic description of fire hazards and their resulting peak thermal exposures for the exposed conduit. Parametric studies are then performed to investigate factors that influence the design targets for thermal exposure, including the tunnel geometry, ventilation condition, conduit installation location, and tunnel traffic. The approach demonstrated in this paper enables stochastic evaluation of thermal loading on exposed conduits based on their placement within the tunnel, traffic content and volume, the tunnel dimensions, and the roadway's accident rate. The results provide a means to determine performance thresholds for fire testing toward continued operability of electrical systems in terms of either a fire return period or the probability of exceedance for a given hazard intensity.

1.2. Existing fire resistance

As shown in Table 1, standards or specifications associated with fire resistance of tunnel conduit piping can be divided into two categories: conduit combustibility, and conduit functionality. Conduit combustibility is addressed by NFPA 130 (Standard for fixed guideway transit and passenger rail systems) as noted in its 2007 edition (Guo et al. 2019): "*material manufactured for use as conduits, raceways, ducts, boxes, cabinets, equipment enclosures, and their surface finish materials shall be capable of being subjected to temperatures up to 500°C (932°F) for 1 hour and shall not support combustion under the same temperature conditions*". In subsequent editions of NFPA 130 (National Fire Protection Association 2010, 2020), non-combustibility of the materials is determined in accordance with ASTM E136 (ASTM International 2019), which restricts the temperature increase to no more than 1°C in any one minute period when exposed to a 750°C furnace fire demand. For the electrical conduit functionality under fire hazard, UL 2196 requires the circuit to maintain signal connection after exposure to 1000°C (1850°F) for 2 hours.

ASTM E1529 (Standard test method for determining the effects of large hydrocarbon pool fires on structural members and assemblies) (ASTM International 2016) can also be applied to electrical conduits, as noted in the standard: "*this test method is intended to provide a basis for evaluating the time period during which a beam, girder, column, or similar structural assembly, or a nonbearing wall, will continue to perform its intended function when subjected to a controlled, standardized fire exposure*." Acceptance criterion are only defined for determining the fire-containment capability of walls, but the prescribed time history for thermal exposure can be readily applied to other systems to achieve user-defined thermal resistance objectives for other components. The ASTM E1529 thermal exposure is provided both in terms of temperatures and heat flux as shown in Table 1.

Table 1: Existing standard testing methods for conduit

Non-combustibility of conduit pipe			
Standard		Temperature (°C)	Duration (hours)
NFPA 130 (Version 2007) (National Fire Protection Association 2007 p. 130)		500	0.50
NFPA 130 (Version 2010 through 2020) (National Fire Protection Association 2010, 2020)		750	1
Functionality subjected to fire hazard			
Standard		Temperature (°C)	Duration (hours)
UL2196 (UL Standard 2017)		1000	2
ASTM E1529 (ASTM International 2016)	Lower bound	1010	N/A
	Mean value	1095	
	Upper bound	1180	
Standard		Heat flux (kW/m^2)	Duration (hours)
ASTM E1529 (ASTM International 2016)	Lower bound	150	N/A
	Mean value	158	
	Upper bound	166	

1.3. Performance-based approach

1.3.1. CDSF modeling of the fire and heat transfer

The CDSF model calculates the peak thermal impact from a fully developed vehicle fire that is enclosed in the tunnel. The development of this model and the validation process has been detailly introduced in the Report Year 3 Task 2. Here, for the integrity of the article logic, a brief introduction is provided. For more details, please refer to the aforementioned report.

For the CDSF model application, the fire is assumed to be distant from the portals such that the openings to the outside do not significantly influence the fire development or airflow. The fire is also assumed to be located at the center of the tunnel width as a symmetric simplification for the confinement fire and the resulting heat exposure effects. The flames are represented as a solid 3D object that radiates emissive power

to the exposed tunnel surfaces, while the convective heat flux to those surfaces from the hot gases and smoke is represented as a longitudinally and radially decaying field. The end result of a CDSF calculation is the spatial distribution of total heat flux (kW/m^2) over the discretized interior surface of the tunnel liner. For a given fire scenario, the footprint of the CDSF model is represented as an equivalent hydrocarbon pool fire and uses diesel fuel as a basis to provide the same heat release rate as the predefined vehicle fire scenario. The fully developed vehicle fire intensity is expressed as maximum heat release rate (HRR), $\dot{Q}_{f,max}$ (kW) per Eq. (1):

$$\dot{Q}_{f,max} = \Delta H_{c,eff} A_{f,eff} \left[\dot{m}''_{\infty} (1 - e^{-k \cdot D_{f,eff}}) \right] \quad (1)$$

where for the selected fuel, $\Delta H_{c,eff}$ (kJ/kg) is the effective heat of combustion; $\dot{m}''_{\infty}$ (kg·m^{-2}·sec^{-1}) is the maximum mass loss rate per unit area; and $k\beta$ is an empirical value that equals the product of the extinction coefficient, k (m^{-1}), and dimensionless mean-beam-length correction, β; and $D_{f,eff}$ (m) is the effective diameter of the pool fire which is used as basis for all geometric parameters (e.g., flame height, flame drag, and radiative fraction). $A_{f,eff}$ (m^2) is the area of the footprint calculated via Eq. (2):

$$A_{f,eff} = \pi \frac{D_{f,eff}^{\ 2}}{4} = L_f \cdot W_f \quad (2)$$

where L_f (m) and width W_f (m) are the equivalent length and width of the rectangular vehicle fire. For a selected $\dot{Q}_{f,max}$, Eq. (1) is iteratively solved to obtain the equivalent diesel footprint dimensions. The aspect ratio (L_f/W_f) is defined as 2.0 for fire intensities less than or equal to 200 MW and as 2.5 for greater intensities (McGrattan et al. 2000). To avoid potential "blind spots" at the corners of a box-shaped model, the rectangular footprint is converted to an ellipse with the same perimeter.

The first iteration of the CDSF model considered naturally ventilated conditions (Guo et al. 2019). However, longitudinal ventilation systems are often used in modern tunnels to remove smoke, aid egress, and assist emergency response and firefighting by creating a smoke-free region upstream of the fire. Per NFPA 502 (NFPA 2017 p. 502), longitudinal ventilation systems are typically designed to operate during a fire event at a calculated critical airflow for a given tunnel geometry. The second generation CDSF model was thereby developed to account for the wind-tilt effects of longitudinal airflow at critical velocity (Zhu et al. n.d.). Critical velocity for longitudinal airflow to prevent smoke backlayering during a fire is correlated with fire intensity and tunnel geometry. For this study, the theoretical value for critical velocity, u_c (m/s), is calculated using Eq. (3) per the 2017 edition of NFPA 502 (NFPA 2017 p. 502) (based on previous work by Thomas (Thomas 1958, 1968) and Danziger and Kennedy (Kennedy and Lowndes 1996)):

$$u_c = K_g \left(\frac{g \dot{Q}_c H_{T,eff}}{\rho_0 c_p T_f A_T Fr_c} \right)^{1/3} \quad (3)$$

where $\dot{Q}_c$ (kW) is the convective HRR, assumed to be 60-80% (Ingason et al. 2015a) of the total heat release rate $\dot{Q}_{f,max}$ (a median value of 70% is applied in this study); $H_{T,eff}$ (m) represents the effective tunnel height, which measures the distance from the base of the fire source to the highest point of the tunnel ceiling ($H_{T,eff} = H_T - H_{base}$) ; ρ_0 (kg/m^3), c_p (kJ/kg-K), and T_0 (K) are the density, specific heat, and temperature of ambient air, respectively; A_T (m^2) is the cross-sectional area of the tunnel; and g(m/s^2) is the acceleration of gravity. Critical Froude number Fr_c can vary from 4.5 to 6.7 based on experiments by Lee et al. (LEE et al. 1979) – in this study, a conservative value of 4.5 is applied for a large tunnel fire. The average downstream temperature T_f (K) is expressed as:

$$T_f = \frac{\dot{Q}_c}{\rho_0 c_p A_T u_c} + T_0 \tag{4}$$

and K_g is a coefficient that accounts for the effect of the tunnel's grade (expressed as a percentage):

$$K_g = 1 + 0.0374(grade)^{0.8} \tag{5}$$

It should be noted that the current formulation of the CDSF model assumes zero (i.e. flat) grade as a simplification. Incorporation of grade in a naturally ventilated scenario will introduce longitudinal asymmetry for convective effects as well as a slight flame tilt in the uphill direction. Grade effects will be similar but much less significant for the longitudinally ventilated scenario due to the influence of the forced airflow. Grade affects will be the subject for future work on the CDSF modeling approach; however, all prototype tunnels examined in this study will be assumed to have zero grade.

The process to forming the 3D solid flame object for calculating radiative heat flux under naturally ventilated conditions is accomplished in three steps:

(1) Extrude the free flame as an ellipsoid from the previously defined footprint, using semi-empirical flame height calculations per Heskestad (Heskestad 1983). The base of the extruded solid flame is elevated to represent an associated vehicle bumper height. The free solid flame object resulting from Step 1 consists of an ellipsoid body and a domed top. The radiative emission from the free flame object is assumed to be evenly distributed over its surface and is calculated as a fraction of the fire's peak heat release. If the free flame height is less than the tunnel ceiling height, then skip to Step 3.

(2) *If the free flame height exceeds the tunnel ceiling height*, confine the free flame considering the enclosure of the tunnel. As the fire size grows, the dome portion (shaded red in Figure 1a) is confined first – for larger fire sizes, the confinement is also extended to the ellipsoid body (shaded yellow in Figure 1a). In the confinement process, the emissive power of each portion (dome and body) is increased proportionally to its decrease in surface area, thus preserving the total radiative energy from the solid flame object.

(3) *If longitudinal ventilation is applied at critical velocity*, apply wind tilt and flame drag in the airflow direction. The resulting solid flame shape will become warped as shown in Figure 1b.

The details for implementing these steps are provided in the authors' previous work (Guo et al. 2019). Once the solid flame object is formed, its surface is discretized into rectilinear elements, each of which emits radiation normal to its surface. Again based on the authors' previous work (Guo et al. 2019), the flame surfaces for this study are discretized to approximate squares with 0.25m maximum edge dimension. The radiative heat flux on the discretized interior surface of the tunnel liner (rectilinearly discretized to 1m maximum edge dimension) can then be calculated as a summation of the contributions from all the discretized flame surfaces that can "see" the target, as expressed in Eq. (6) and illustrated in Figure 1a:

$$\dot{q}''_{rad,j} = \sum_{i=1}^{n} E_i F_{i\to j} = \sum_{i=1}^{n} E_i \frac{A_i cos\theta_i cos\theta_j}{\pi r_{i\to j}^2} \tag{6}$$

where E_i (kW/m^2) and A_i (m^2) are the emissive power and the area of the i^{th} element on the fire surface, respectively; $r_{i\to j}$ is the distance or "radius" from the center of fire surface element i to target element j; θ_i represents the absolute angle in 3D space between the radius vector and the fire element's normal vector; and θ_j is the absolute angle in 3D space between the radius vector and the target surface normal vector.

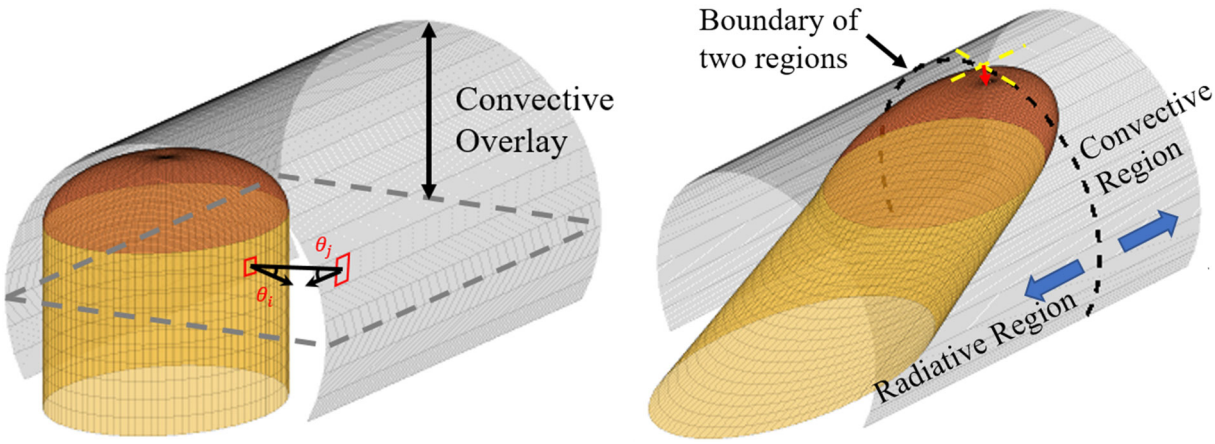

(a) Naturally ventilated CDSF model (b) Longitudinally ventilated CDSF model

Figure 1: CDSF model illustration within a circular tunnel cross-section

The calculation of convective heat flux at peak fire conditions is based on a combination of semi-empirical measurements and numerical CFD simulations. For a naturally ventilated case, the hot gases and smoke are symmetrically distributed along the longitudinal axis and along the section height. The maximum convective heat flux directly above the fire is calculated with Eq. (7) as follows. A minimum value of 3 kW/m^2 is imposed as a lower bound floor to the logarithmic function, thus preventing artificially low predictions of convective heat flux for smaller fires (i.e., with HRR below 30 MW).

$$\dot{q}''_{c,max} = \max[3, 68\ln(\dot{Q}_{f,max}) - 702] \tag{7}$$

Then, separate decay expressions are applied in the longitudinal direction (away from the fire location) and vertical direction (from the ceiling downward) to account for decreasing concentration and temperature in the smoke and other combustion byproducts. The peak convective heat flux is calculated as a function of fire intensity in terms of peak HRR. The convective heat flux values at every discretized target on the interior surface of the tunnel liner are then added to the radiative contributions from the solid flame object to obtain total heat flux. Figure 2a provides an example of the heat flux distribution at peak conditions on a three-lane circular tunnel subjected to a vehicle fire of 100 MW in the case of natural ventilation.

For longitudinally ventilated conditions, the 3D field of smoke and hot gas are pushed downstream of the fire by the airflow at critical velocity, thus leaving the upstream region clear for only radiative heat flux from the solid flames. In this case, the convective region begins at the longitudinal location of the flame dome's center, as shown in Figure 1b, and then decays in the downstream direction. The same vertical decay approach from the naturally ventilated case is used here in the convective region. Using the same three-lane circular tunnel as for the natural ventilated case, the total heat flux contour for a 100 MW fire with longitudinal ventilation at critical velocity is plotted in Figure 2b.

For the case of a three-lane circular tunnel subjected to a 100 MW fire, Figure 2 shows that the maximum heat flux values for longitudinal ventilation at critical velocity are ~50% lower than those for the naturally ventilated case. However, the longitudinal airflow produces a more widespread distribution of heat flux over the tunnel liner surface. The resulting distribution of fire-induced damage will depend on both the intensity and distribution of total heat flux. The results of this study will highlight these differences between natural and longitudinal ventilation cases when examining the thermal impact onto conduit piping that is mounted to the interior face of the liner. For simplicity, the total heat flux experienced by the conduit is assumed to be the same as that experienced by the liner at the same location per the CDSF model.

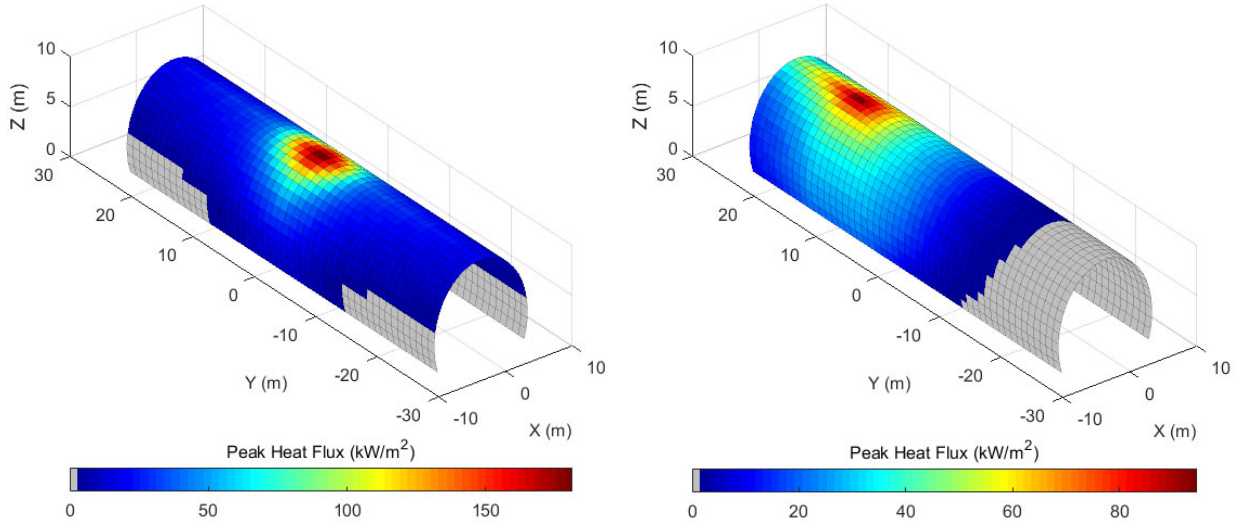

(a) Natural ventilation (b) Longtidinal ventilation

Figure 2: Illustrative examples of total heat flux from the CDSF model for a 100MW fire within a 2-lane circular tunnel cross-section

1.3.2. Design fire time history

The time history of total heat flux (radiation plus convection) that is imparted to every discretized location on the tunnel liner can be assumed to follow the same ramp-up, peak duration, and decay as the fire's HRR. This study adopts Ingason's quadratic design curve for tunnel fires (Ingason 2009), which consists of a quadratic growth phase, a constant steady-state peak phase, and an exponential decay phase per the following equations:

$$\dot{Q}_f(t) = \begin{cases} \alpha_{g,q} t^2 & , \ t \le t_{max} \\ \dot{Q}_{f,max} & , \ t_{max} < t < t_D \\ \dot{Q}_{f,max} e^{-\alpha_{D,q}(t-t_D)} & , \ t \ge t_D \end{cases} \quad (8)$$

$$t_{max} = \sqrt{\dot{Q}_{f,max}/\alpha_{g,q}} \quad (9)$$

$$t_D = \frac{\chi E_{tot}}{\dot{Q}_{f,max}} + \frac{2}{3} t_{max} - \frac{1}{\alpha_{D,q}} \quad (10)$$

where E_{tot} (kJ) is the total combustion (or calorific) energy; χ is the combustion coefficient (conservatively taken as 1.0); $\alpha_{g,q}$ (kW/s^2) and $\alpha_{D,q}$ (s^{-1}) are the quadratic growth and exponential decay rates, respectively (which are related to the vehicle or fire type (Ingason 2009)). The duration of steady state HRR at $\dot{Q}_{f,max}$ is directly related to E_{tot}; therefore, data was collected from the results of previous tunnel fire tests with varying vehicle types, sizes, and different payloads (see

Table 2) and plotted in Figure 3 to obtain the following regression equation:

$$E_{tot} = 3.31 Q_{max}^{1.066} \quad (11)$$

Table 2: Summary of combustion energy and peak HRR from the results of published fire tests

Combustible content involved	Estimated combustible weight (kg)	Theoretical calorific energy (GJ)	Estimated peak HRR (MW)	Source
2-3 cars	N/A	17	8	(Ingason 2009)
Van		38	15	
HGV: no "hazardous good"		144	30	
HGV: with "high calorific potential"		450	100	
Fuel Tanker		960	200	
Multiple HGVs	71630	1500	370	(Lönnermark 2005)
Multiple HGVs with multiple cars	102431	2145	380	

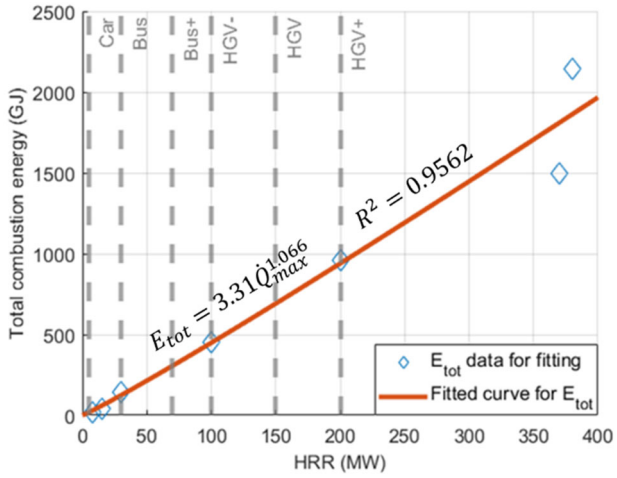

Figure 3: Total combustion energy for tunnel fires as a function of peak HRR

The 2017 edition of NFPA 502 (NFPA 2017) groups vehicle fires in tunnels into four basic categories with associated peak HRR, which are summarized in Table 3: passenger car, bus, HGV, and fuel tanker. Each type is assigned a typical peak HRR to represent the fire intensity. Based on the experimental ranges reported in NFPA 502 (NFPA 2017) and by Ingason (Ingason 2009), an additional "Bus+" case at 70 MW and upper/lower bound for HGVs at 100 and 200 MW are selected to create a broader spectrum of peak HRR for the evaluation in this study (as plotted with the gray dashed lines in Figure 3). The fuel tanker fire case is not included in this study because preliminary analyses indicated that a fire of this size would impart extensive structural damage to the tunnel liner, thus making a thermal evaluation of mounted conduit piping somewhat irrelevant since it would also experience total detachment from the liner.

Table 3: Peak HRRs of vehicle fires used for analysis in this study

Vehicle Type	**Representative HRR** (NFPA 2017) **(MW)**	**Selected HRR (MW)**	**Recommended growth rate** $\alpha_{g,q}$(kW/s^2);	**Recommended decay rate** $\alpha_{D,q}$(s^{-1})
Passenger Car	5	5	0.01	0.0010
Bus	30	30, 70	0.10	0.0007
HGV	150	100, 150, 200	0.30	0.0010
Fuel Tanker	300	N/A	N/A	N/A

The resulting HRR time history curves for vehicle fires ranging from passenger cars to HGVs are plotted in Figure 4. The duration of steady-state peak HRR ranges from 41 to 58 minutes for all fire cases in this study, and the total duration of thermal exposure does not exceed 2.5 hours. Based on these results, the practical bounds of the peak duration of thermal exposure for a standard test could range from 30 minutes to 2 hours, depending on a user-defined threshold of fire hazard severity.

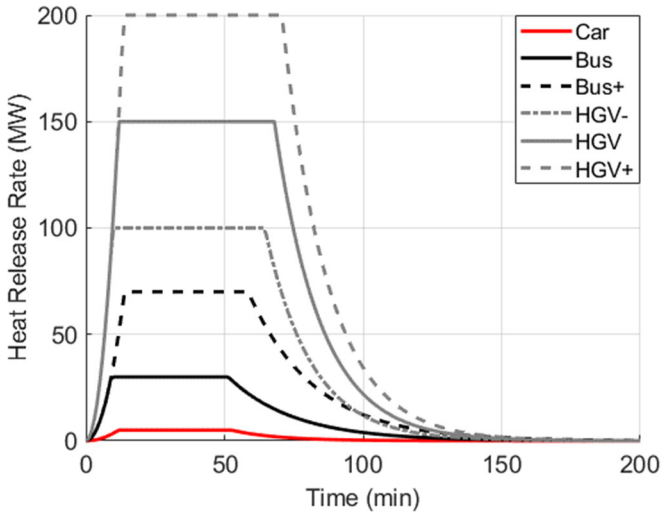

Figure 4: HRR time histories considered for this study

1.3.3. FE thermal analysis of the conduit

The thermal response of the fire exposed conduit is analyzed via finite element analyses in SAFIR (version 2019) (Franssen and Gernay 2017). The cross-section of the conduit is discretized into 2D solid fibers as illustrated in Figure 5, with four evenly spaced fibers in the radial direction through the conduit wall and thirty-six evenly spaced fibers in the circumferential direction. The outside surface of the conduit is assumed to be exposed to thermal demand in terms of either temperature or heat flux. To consider the uncertainty in the orientation of the enclosed fire effects relative to the conduit, different surface heating percentages are implemented in the model. For example, a fully engulfed conduit pipe is considered to have 100% surface exposure as shown in Figure 5a. If a conduit section is located far from the fire and is only subjected to exposure on one face, then 50% conduit surface exposure would be assumed.

The cavity of the conduit is simplistically modeled as void space. The material of the conduit in this study is either rigid galvanized steel (RGS) or stainless steel (SS), which are modeled as STEELEC3 and SLS1.4401 in SAFIR (Franssen and Gernay 2016), respectively. The temperature-dependent thermal properties including thermal conductivity and specific heat of each material follow those specified in Eurocode 3, Part 1-2 (CEN 2005). The convective coefficients for the fire-exposed and unexposed surfaces are taken as 25 kW/m^2 and 9 kW/m^2 per Eurocode 1, Part 1-2 (CEN 2009). The emissivity of RGS and stainless steel are both taken as 0.7, also per Eurocode 1 (CEN 2009).

The steady-state temperature distribution of an example stainless conduit cross-section when exposed to the ASTM E1529 (ASTM International 2016) heat flux time-history curve is presented in Figure 5. A type 316 stainless-steel conduit manufactured in accordance to ANSI C80.1 (ANSI C80.1 2005) with an outside diameter of 26.67mm (1.05 in) and inside diameter of 20.83mm (0.824 in) is selected for this analysis. For the uniform exposure case, the entire cross-sectional temperature rapidly reaches 1077°C

(Figure 5a) while the temperature distribution for the 50% exposure varies from 751°C to 944°C (Figure 5b). The reduction in heating exposure can therefore have a significant influence on the average temperature increase of these conduits.

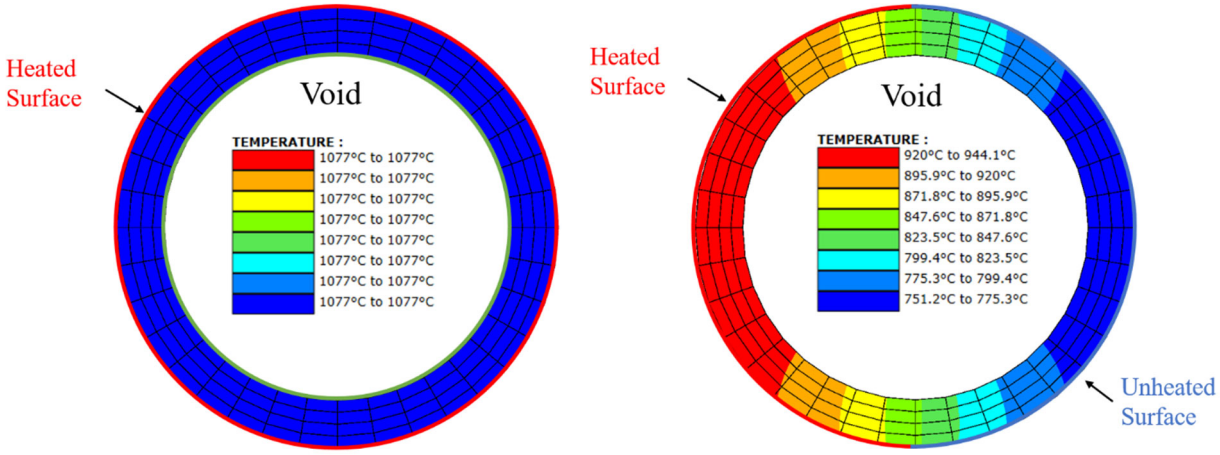

(a) 100% conduit surface exposure (b) 50% conduit surface exposure

Figure 5: SAFIR thermal analysis results for conduit at steady state

The temperature sensitivity of the conduit pipe exposed to fire is investigated relative to the material, pipe sizing, and thermal input type (e.g., temperature or heat flux) in addition to the exposure area. Figure 6 shows the average temperature time history of the interior surface of the conduit during exposure to the ASTM E1529 standard curve. The temperature time history curves for conduit of different material and pipe sizes are plotted in Figure 6a when subjected to a 100% surface exposure of the full heat flux value (blue lines) and half heat flux value (red lines) prescribed by the ASTM E1529 standard. The tightly banded results for each exposure demonstrate that the conduit temperature is not sensitive to pipe material or sizing due to the small thermal mass of the conduit. In Figure 6b, the exposure area is varied when applying either the full prescribed heat flux or temperature from ASTM E1529 (see Table 1). As expected, the 158 kW/m^2 heat flux is essentially equivalent to 1095°C temperature demand for both the 100% and 50% surface exposure cases. The 50% exposure cases result in a 23% reduction in the average interior temperature compared to the 100% exposure cases. Together, the plots in Figure 6 show that the conduit temperature nearly converges to the heating temperature magnitude due to the small thermal mass of the pipe. Consequently, the temperature increase of the conduit can be approximately equated to the thermal exposure. Hence, the conduit temperature reached during a realistic fire exposure could be used to practically indicate the temperature threshold for evaluating the results of a standard fire test.

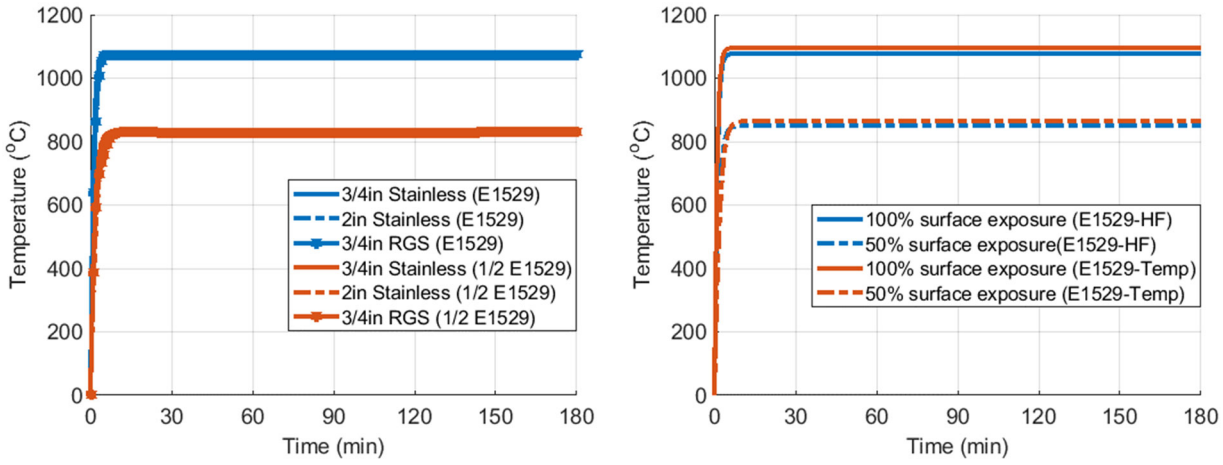

(a) Conduit sizing and material sensitivity (b) Surface exposure percentage sensitivity

Figure 6: Average internal surface temperature time history of typical conduit piping for ASTM E1529 heat flux and temperature demands (ASTM International 2016)

1.3.4. Correlating heat flux exposure to internal conduit temperature

Based on these results, a correlation can be developed to provide a conservative estimation of the average conduit internal surface temperature based on the applied heat flux. A series of thermal analyses were therefore performed in SAFIR to correlate the steady-state conduit temperature with the heat flux at the boundary. As previously illustrated, the maximum internal temperature is not sensitive to typical conduit sizing and material. A type 316 stainless-steel conduit manufactured in accordance with ANSI C80.1 (ANSI C80.1 2005) with an outside diameter of 26.67 mm (1.05 in) and inside diameter of 20.83 mm (0.824 in) is therefore selected as a representative case for this analysis. The thermal load is varied from a heat flux of 10 kW/m^2 to 400 kW/m^2 applied to 50%, 75%, and 100% of the outer surface area, and the analysis results are plotted as open circles in Figure 7.

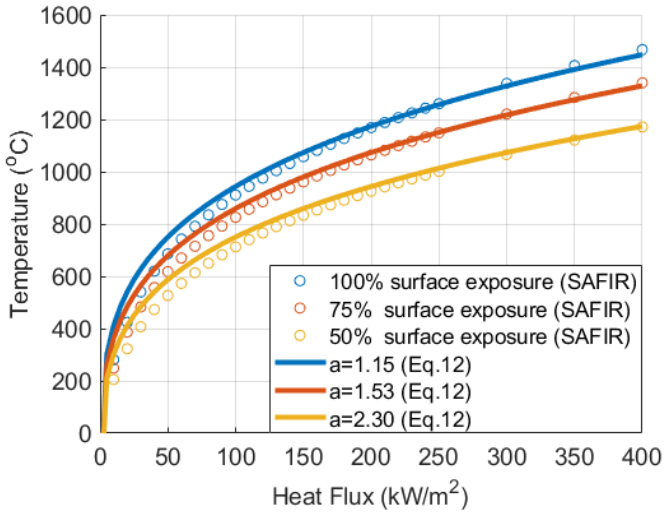

Figure 7: Relationship between average internal conduit surface temperature and applied heat flux

A correlation defined in Eurocode 3, Part 1-2 (CEN 2005) and adopted in a previous study by Zhu et al. (Zhu et al. 2020) is modified here to approximately relate the applied heat flux to the temperature on the fire-exposed surface:

$$T = \left(\frac{\dot{q}^{"}}{\sigma \cdot a \cdot \varepsilon_{in}} \right)^{1/4} - 273 \tag{12}$$

where $\dot{q}^{"}$ (kW/m^2) is the heat flux applied to the fire-exposure surface; ε_{in} is the resultant emissivity (set at 0.7 for stainless steel per Eurocode 1, Part 1-2 (CEN 2009 p. 1)); σ is the Stefan-Boltzmann constant (5.67E-8 W/m^2-K^4); and a is an amplification factor for calibration (set equal to 1.15/(exposure %); for example, a = 1.53 for the 75% exposure). The curves plotted in Figure 7 show conservative agreement with the thermal FE results, and Eq. (12) will therefore be used in the subsequent parametric study to describe the internal temperature of any generic conduit within the aforementioned sizing range.

1.4. Parametric study for internal conduit temperature

Using the results of the CDSF model as input for Eq. (12), a parametric study is performed to investigate the thermal response of conduits for tunnels of varying dimensions with enclosed fires of varying intensities. In this process, both natural (i.e., zero forced airflow) and longitudinal (airflow at critical velocity) ventilation conditions are considered, as well as the conduit location within the tunnel cross-section and the fire exposure conditions. Note that the vehicle fire is assumed to be located at the transverse center of the tunnel, which is inherent to the current formulation of the CDSF model (Guo et al. 2019; Zhu et al. 2022) and reflective of most large-scale fire tests in the current literature (Bechtel/Parsons Brinckerhoff. and Bechtel/Parsons Brinckerhoff. 1995; Ingason et al. 2011). Future work should examine potential variations in thermal exposure (particularly on sidewall locations) that result from an off-center

fire footprint location. However, most large fires within a tunnel have very small standoff to the sidewalls regardless of their transverse location, and the resulting change in heat flux at these locations would therefore not alter the overall conclusions of this study.

1.4.1. Analysis matrix

According to a previous investigation (Guo et al. 2019), tunnels in the US typically have a road width ranging from 8-13m, accommodate 2 to 3 lanes, and have a curved ceiling (i.e. with either a circular or horseshoe shaped cross-section). Due to the development of tunnel boring machines, the circular tunnel cross-section is becoming increasingly common among newer tunnel construction (Guo et al. 2019). This study therefore focuses on circular tunnels with either 2- or 3-lanes of traffic as shown in Figure 8. Two linearly interpolated tunnel sizes are considered for each lane width to develop a reasonable spectrum of response. The selected fire intensities are based on the vehicle fire categories per NFPA 502 (NFPA 2017) and are consistent with the tunnel fire design curve analysis presented previously in Section 1.3. Three locations around the inner circumference of the tunnel cross-section in Figure 8 are considered when evaluating the conduit for fire exposure: the top of the tunnel ceiling (horizontal surface), the sidewall (vertical surface), and between the two at sidewall Location 1 (i.e. at half of the arc length between the first two locations). As a simplification, the heat flux applied to a conduit pipe at a given location is taken from the discretized CDSF liner element on which it is installed. Moreover, since the assumed exposure area of the conduit directly influences the resulting conduit temperature as shown in Sections 1.3.3 and 1.3.4, a range of exposure percentages from 50% to 100% are examined. Table 4 provides a full summary of the parameters considered for this study.

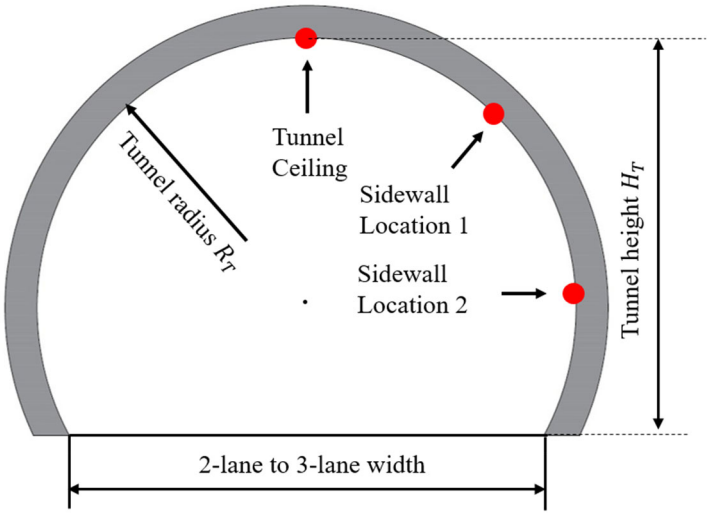

Figure 8: Cross-sectional locations for conduit pipe installation

Table 4: Parametric matrix for evaluating conduit response to fire

Tunnel Parameters		
Dimension		
Radius R_T (m)	Tunnel height H_T (m)	
6.98	9.57	
6.41	8.98	
5.85	8.38	
5.28	7.78	
Ventilation Conditions		
Natural ventilation	Longitudinal ventilation	
Fire Intensity		
Car	Bus	HGV
5MW	30 MW, 70MW	100, 150, 200 MW
Conduit Location		
Ceiling	Sidewall	
Conduit Exposure Area		
50%	75%	100%

1.4.2. Conduit location and exposure percentage

As shown previously in Figure 2, the maximum demands from the enclosed fire will be located at the top of the tunnel ceiling, and the naturally ventilated cases will have a higher maximum total heat flux than longitudinally ventilated cases (at critical airflow velocity) for the same HRR. For reference, the maximum heat flux from CDSF analysis of the vehicle cases, tunnel sizes, and ventilation conditions listed in Table 4 are plotted in Figure 9a. The longitudinally ventilated cases show significantly less variation with changes in tunnel size – the influence of confinement on the CDSF model's solid flame shape will be less significant for these cases because the wind tilt and flame drag elongate it in the downstream direction. Note that the calculated heat flux from the CDSF model is capped at 400 kW/m^2 based on the results of the Runehamar tunnel fire tests by Ingason. et al. (Ingason et al. 2015b). During that test program, a 400 kW/m^2 maximum incident heat flux was measured at the top-of-ceiling in the 5.8-m tall tunnel for a 206 MW enclosed fire, which just exceeds the highest fire intensity in this parametric study.

The internal temperature of the conduit in Figure 9b is calculated using Eq. (12), assuming 100% conduit surface exposure for each maximum heat flux from Figure 9a. The curves in red and blue represent natural and longitudinal ventilation cases, respectively. As shown previously in Section 1.3, the internal conduit temperature when subjected to these fire hazards is essentially equivalent to the thermal exposure, which could then be used as a benchmark for design via a standard fire test. For example, Figure 9b shows that the 1000°C exposure temperature benchmark from UL2196 (UL Standard 2017) (summarized previously

in Table 1) would only be conservative for fire sizes below the Bus+ case in a longitudinally ventilated tunnel (with the wind speed at the critical velocity) and for passenger car fires in the naturally ventilated tunnel. To maintain functionality when subjected to larger fires in this spectrum, an electrical conduit would need to be rated for exposure to a temperature greater than 1000°C for a specified duration (which can range from 30 minutes to 2 hours for these realistic fire cases as shown previously in Section 1.3.2).

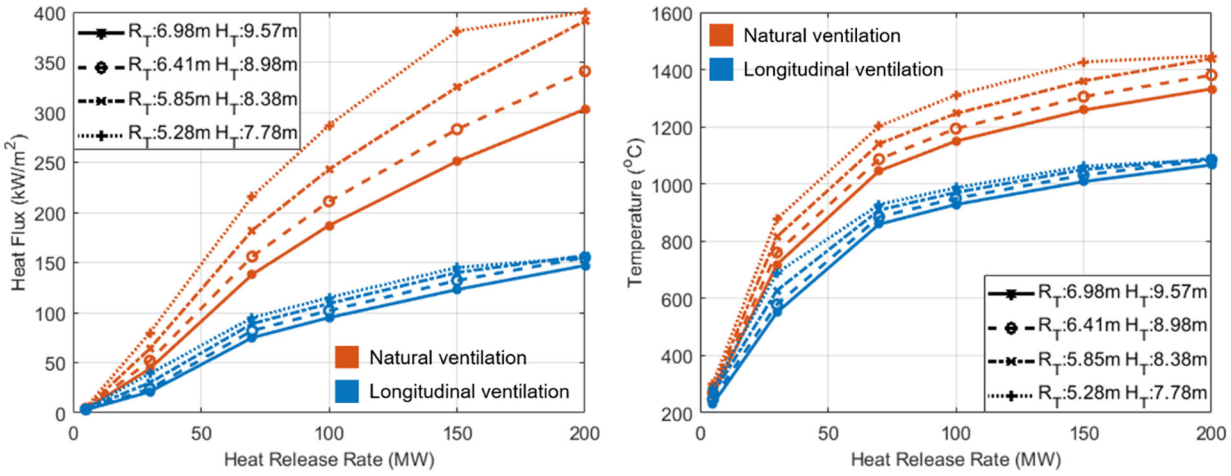

(a) Peak heat flux from CDSF (b) Internal conduit temp. (100% exposure)

Figure 9: Maximum thermal load on the conduit at the top of the tunnel ceiling

Figure 10 and Figure 11 show that the internal temperature in the conduit also decreases significantly when its installed location is shifted downward from the top of the ceiling to Sidewall Locations 1 and 2 per Figure 8. Placement of the conduit closer to the ground results in lower thermal demands by progressively avoiding the maximum radiative and convective impacts from the fire (see Figure 2). As expected, Figure 12 shows that the average internal conduit temperature dramatically decreases when the exposure percentage is reduced. Based on these results, the thermal impact on exposed electrical conduit can be quantifiably reduced by (1) implementing longitudinal ventilation at critical velocity, (2) reducing the exposure surface area, and (3) relocating the installed location from the ceiling to the sidewall. For a given tunnel configuration and expected fire exposure, the results in Figure 9 through Figure 12 can serve as a useful tool for determining the temperature at which a conduit should be tested to remain functional when subjected to particular fire intensity. To properly leverage these results in practice, further experimental testing is needed to determine the appropriate exposure percentage for a given fire, tunnel, and conduit configuration. A user could then implement the CDSF modeling approach and Eq. (12) to determine an appropriate temperature threshold at which a conduit should be rated to preserve functionality during an actual fire.

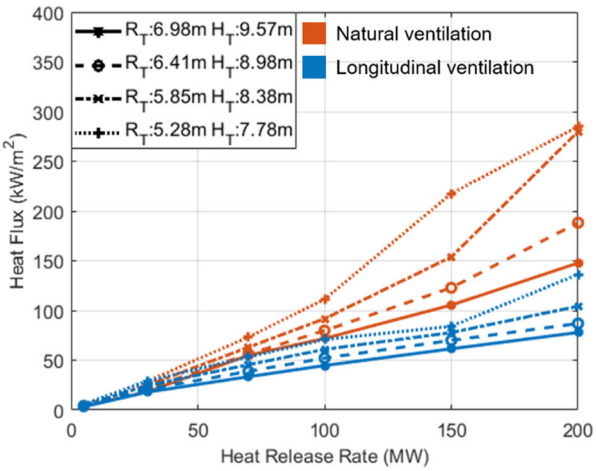

(a) Peak heat flux from CDSF

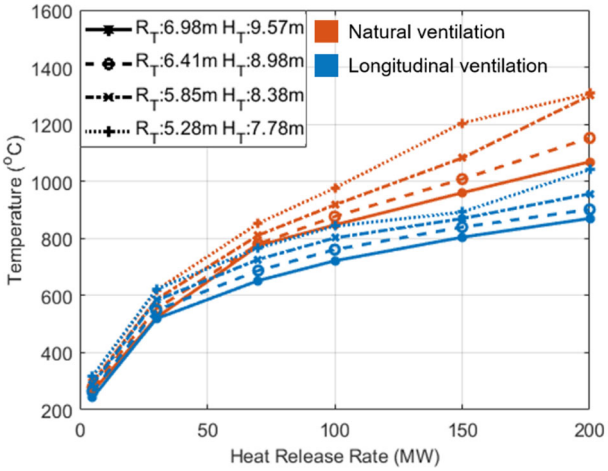

(b) Internal conduit temp. (100% exposure)

Figure 10: Maximum thermal load on the conduit at Sidewall Location 1 per Figure 8

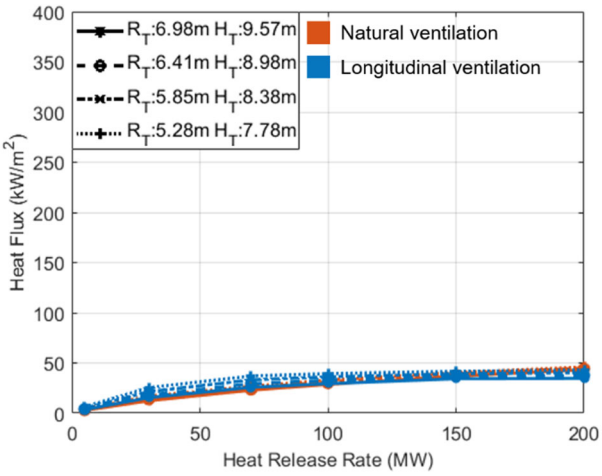

(a) Peak heat flux from CDSF

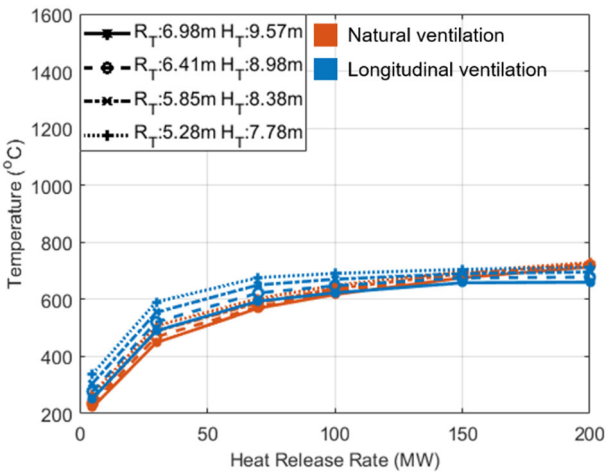

(b) Internal conduit temp. (100% exposure)

Figure 11: Maximum thermal load on the conduit at Sidewall Location 2 per Figure 8

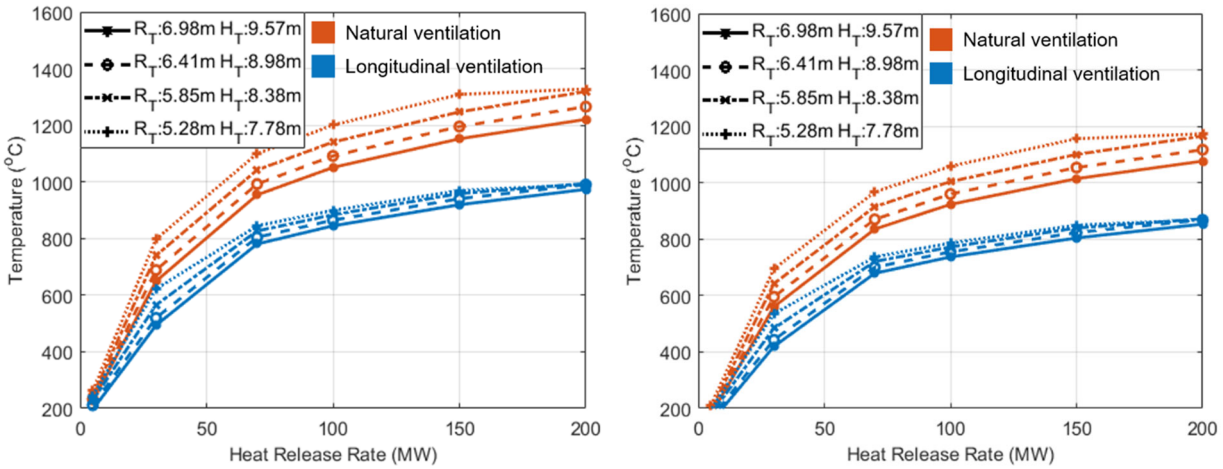

(a) 75% surface exposure (b) 50% surface exposure

Figure 12: Internal conduit temperature at the top of the tunnel ceiling for varying exposure percentage

1.5. Thermal threshold selection based on tunnel traffic

The results in Section 1.4 show that current prescriptive fire resistance metrics for electrical conduits in tunnels (summarized in Section 1.2) may not necessarily ensure continued functionality when subjected to the range of fire intensities specified in NFPA 502, depending on the ventilation conditions, tunnel size, and the conduit's exposure to fire. Due to the importance of continued operation of a tunnel's electrical systems during an emergency, the thermal performance rating for these conduits could instead be formulated as a risk tolerance by combining the results of Section 1.4 (which correlate tunnel configuration and conduit exposure to thermal response) with traffic data (which can be used to quantify the fire hazard probability).

The fire frequency, F_f, within a specified time frame in a given tunnel can be calculated via Eq. (13) by multiplying the fire rate R_f (per million vehicle-km), tunnel traffic volume D (total number of vehicles across all types) within that time frame, and tunnel length L (in km):

$$F_f = R_f \cdot D \cdot L \tag{13}$$

A demonstration of Eq. (13) is developed using available data for its three input parameters, which are summarized in Table 4. A tunnel fire rate R_f of 9.6 per million vehicle-km is based on a study published in 2016 by PIARC (PIARC Technical Committee 3.3 2016) for tunnels in eight counties (Guo et al. 2021b). The traffic volume D is taken as an annual average daily traffic (AADT) of 103473 vehicles per day, measured in 2019 for a 2-lane urban tunnel in Pennsylvania, USA, and provided to the research team by collaborators at the Pennsylvania Department of Transportation (PennDOT) (Guo et al. 2021b). The length of this particular tunnel in Pennsylvania is specified as 1219 m (4000 ft). The resulting fire frequency F_f

on an annual basis is 0.44 fire events per year, which can be extrapolated to 22 fire events over a fifty-year duration (with the simplifying assumption that AADT and R_f are unchanged during that period).

A breakdown of traffic composition for the prototype tunnel was also provided by PennDOT (Guo et al. 2021b) and is summarized in Table 5. The HGV vehicle type is subdivided into six categories according to the number of axles. The combustion for each vehicle type is assumed to vary from a lower bound of 30% of the vehicle tare weight up to an upper bound equaling the full payload capacity of the vehicle plus 30% of the tare weight. These weights are also summarized in Table 5 and are assumed to have a normal distribution with the mean value at the average of the lower and upper bound of the combustion weight. The standard deviation for these distributions is set at one-third of the difference between the mean value and upper/lower bound. This ensures that 99.7% of potential fire scenarios will fall within the aforementioned ranges.

To estimate the fire intensity of each vehicle type, a correlation is developed between the combustion weight and HRR based on the fire tests. A curve fit function that relates the $\dot{Q}_{max}$ (MW) and combustion weight *m* (kg) was previously developed by Guo et al. (Guo et al. 2021b):

$$\dot{Q}_{max} = \frac{a \cdot m}{b + m} \tag{14}$$

with dimensionless coefficients a = 441.3 and b = 14830. Similar to the combustion weight assumption, the peak HRR calculated with Eq. (14) follows a normal distribution with the max and min values at three standard deviations from the mean. The results are also summarized in Table 5.

Table 5: Breakdown of tunnel traffic composition, representative combustion weight, and peak fire HRR by vehicle type (Guo et al. 2021b)

Vehicle types	Percent of tunnel vehicle fires	Combustion Weight (kg)		Peak HRR (MW)	
		Mean	Std. Dev.	Mean	Std. Dev.
Motorcycle	0.351%	145	30	4	1
Car	79.053%	1143	272	32	7
Pick-up Truck/Van	13.993%	1977	514	52	11
Bus	0.990%	9283	2748	170	23
HGV (2 Axle)	2.723%	7923	2294	154	22
HGV (3 Axle)	0.908%	12200	3545	199	23
HGV (4 Axle)	0.209%	14803	4027	220	21
HGV (5 Axle)	1.729%	16327	4535	231	21
HGV (6 Axle)	0.041%	16327	4535	231	21
HGV (7 Axle)	0.003%	16327	4535	231	21

The probabilistic distributions in Table 5 are used to develop a continuous cumulative density function relative to peak HRR, which is accomplished by generating one million stochastic HRR samples via Monte Carlo Simulation. The cumulative probability of a specific HRR value is calculated by dividing the number of samples below this HRR by the total number of samples. The resulting cumulative probability relationship for the prototype tunnel with the vehicle distributions in Table 5 is plotted in Figure 13 as a solid black line (denoted in the legend as "HGV percentage = 5.6%"). The cumulative probability increases dramatically from HRR of 5 MW (passenger cars) to 70 MW (Bus+) and then gradually increases across the HGV spectrum. The probability of producing a 100 MW fire hazard is just below 10% while exceeding a 300 MW fire is almost zero.

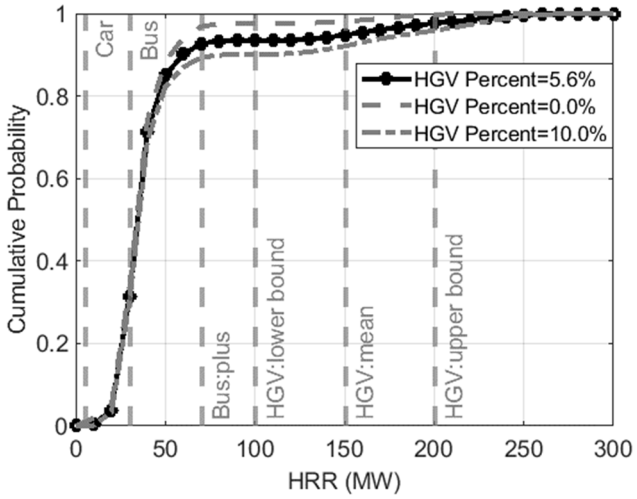

Figure 13: Cumulative probability of tunnel fire intensity in terms of HRR

The fire frequency associated with each type of vehicle can be calculated by combining the overall fire frequency for the prototype tunnel in Table 5 with the cumulative probability shown in Figure 13. For instance, the probability of exceeding a 150 MW HGV fire is 5.22% per Figure 13. The resulting HGV fire frequency would therefore be 0.0230/year (e.g., multiply the fire frequency 0.44/year by 5.22%). The return period for this HGV fire is 43.5 years. Following this procedure, the probability of exceeding a given temperature in the conduit if a fire was to occur can be determined by using fire HRR as input for the CDSF model (per Sections 1.3.1 and 1.3.2) for a given tunnel and conduit configuration (as demonstrated in Section 4.2). The peak conduit temperature at the top-of-ceiling for 100% exposure is plotted in Figure 14a for the four tunnel geometries from Table 4 with and without longitudinal ventilation as a function of the expected return period. Based on this figure, a peak temperature of 1095°C (consistent with the mean prescribed value in ASTM E1529) could be chosen as a functional rating threshold for a 50-year return period for electrical conduits located at the top-of-ceiling in the tunnel geometries with longitudinal ventilation at critical velocity. Similarly, a 1500°C threshold should be applied if natural ventilation is considered for a 50-year return period. If the design return period is reduced to 20 years, the corresponding temperature demands decrease to 1150°C and 900°C for natural and longitudinal ventilation cases, respectively.

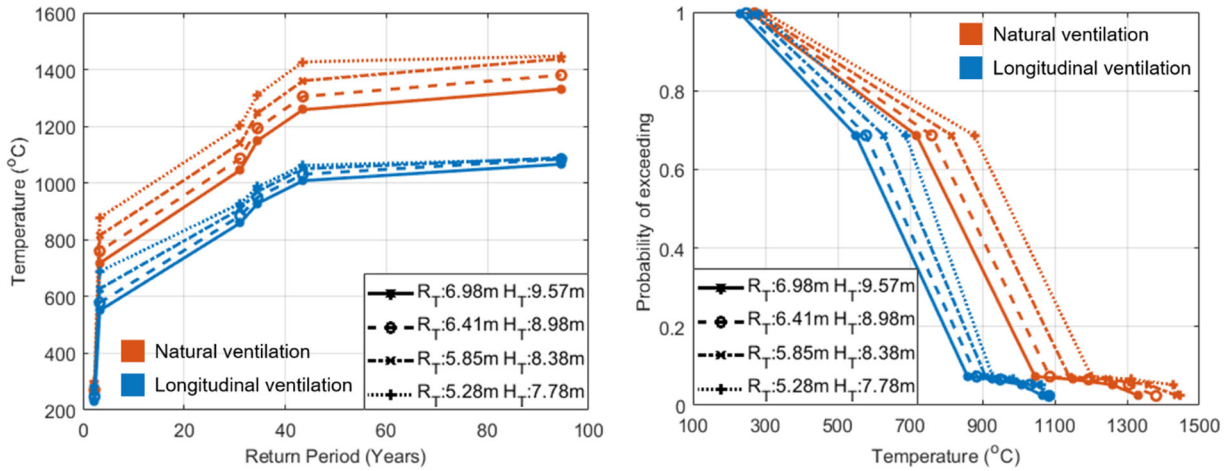

(a) As a function of expected fire return period (b) Probability of exceedance

Figure 14: Maximum internal conduit temperature thresholds based on fire hazard and traffic data

Alternatively, the temperature threshold can be based instead on the probability of exceedance. For example, for a given tunnel fire event, the 1000°C temperature benchmark applied in UL2196 would have a 7.5% probability of exceedance for the longitudinal ventilation cases, while the probability would increase markedly for natural ventilation cases, as shown in Figure 14b. Based on this figure, a conduit temperature of ~1250°C could be considered as a practical threshold corresponding to 10% probability of exceedance for natural ventilation cases.

1.5.1. Sensitivity study

As demonstrated above, tunnel traffic plays a prominent role in the probabilistic examination of fire-induced thermal demands for these conduits. A sensitivity analysis is therefore conducted using the parameters summarized in Table 6. The tunnel length and AADT both vary from 50% to 200% versus their original data. Also, the percentage of HGVs (originally at 5.6%) is reduced to 0% and increased to 10%. When the HGV percentage is modified, the percentage of all other vehicle types is adjusted by uniformly redistributing the difference between the updated HGV percentage and the original percentage. For demonstration, the influence of these parameters is examined using the 3-lane prototype tunnel with a tunnel height of 9.57m and radius of 6.98m, as listed in Table 4.

Table 6: Parametric study of tunnel traffic

Traffic composition			Tunnel length	AADT (vehicles per day)
Vehicle type	HGV@0%	HGV@10%		
Motorcycle	1.80%	0.00%	610m (2000ft);	51736 (50%);
Car	80.50%	77.10%		
Pick-up Truck/Van	15.40%	12.90%	1828.5m (6000ft);	155210 (150%);
Bus	2.40%	0.00%	2438m (8000ft)	206499 (200%)
HGV	0.00%	10.00%		

In Figure 15, the influence of AADT and tunnel length in calculating the return period of tunnel fires are equivalent, producing a linearly proportional increase or decrease in the annual fire rate. By reducing the overall traffic volume to 50% of the original value, Figure 15 also shows that the conduit temperature for a 50-year return period decreases by 22% for both the natural and longitudinal ventilation cases compared to the results shown in Figure 14. However, if the traffic is enlarged by 50% or doubled, the conduit temperature only increases to 1350°C (+2.2%) and 1400°C (+6.0%) for natural ventilation cases and to 1100°C (+1.8% increase) and 1150°C (+6.5% increase) for longitudinal ventilation case.

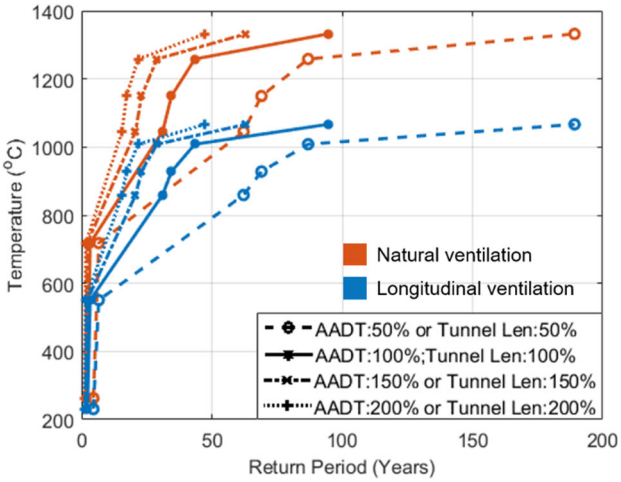

Figure 15: Influence of AADT and tunnel length on maximum internal conduit temperature

For each traffic composition listed in Table 6, one million samples are generated to develop the gray-dashed cumulative probability density curves shown in Figure 13. The influence of varying the HGV percentage in determining the maximum internal conduit temperature is illustrated in Figure 16. Using the 3-lane prototype tunnel with the original traffic composition as the comparison benchmark, eliminating HGV traffic decreases the conduit temperature threshold by approximately 25% for a 50-year return period Figure 16a, from 1080°C to 800°C for the longitudinally ventilated case and from 1320°C to 1000°C for the natural ventilation case. However, the conduit temperature only increases by 2.5% if the HGV percentage is doubled. To obtain the same probability of exceedance at 5% in Figure 16b, the maximum temperature would be 1100°C for the high HGV percentage case and 900°C for no-HGV cases. These

results demonstrate the ability of the proposed performance-based approach to incorporate changes to traffic composition in determining the maximum thermal demand for these conduit pipes as a function of fire hazard probability.

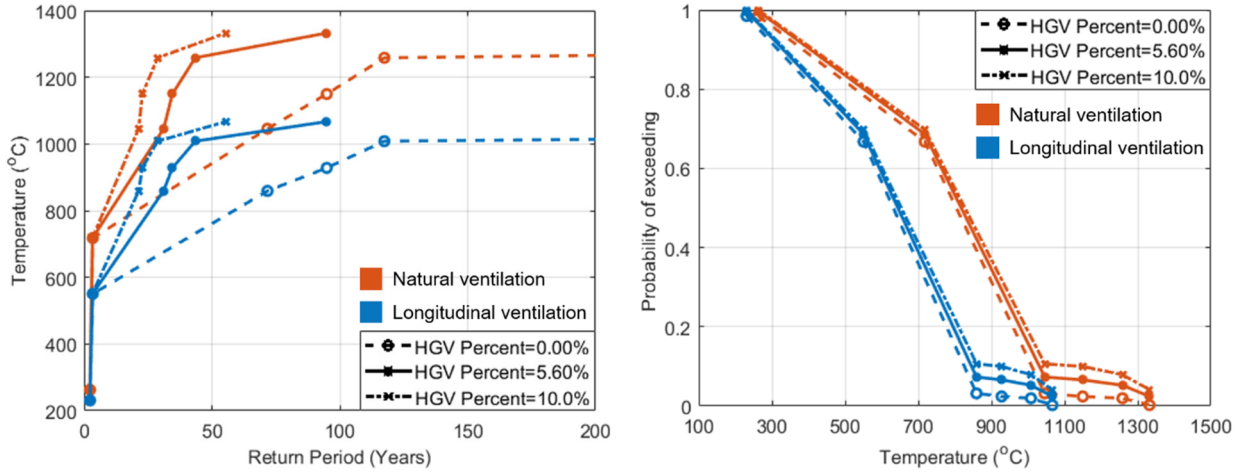

(a) As a function of expected fire return period (b) Probability of exceedance

Figure 16: Influence of HGV traffic percentage on maximum internal conduit temperature

1.6. Conclusions

Vehicle fires in roadway tunnels not only induce structural damage but also threaten the integrity of vital nonstructural components. This paper focuses on the fire resistance of steel electrical conduit, which directly affects the functionality of the lighting, ventilation, and other electrical tunnel systems during a fire event. Thermal demand envelopes are developed for typical conduit pipes based on the magnitude of the fire and the exposure of the conduit pipe at several locations in a prototype circular tunnel cross-section. Multiple sensitivity analyses were conducted to examine uncertainties associated with conduit properties, tunnel geometry, and the fire hazard as a function of tunnel traffic. The conclusions of the study are as follows:

- The confined discretized solid flame (CDSF) model previously developed by the authors can efficiently calculate the incident heat flux on the conduit due to vehicle fires with varying intensities, the range for which is obtained from NFPA 502. Both naturally ventilated and longitudinally ventilated (with airflow at critical velocity) conditions can be considered.
- Due to their small thermal mass, the temperature increases in the conduit pipe when subjected to fire is not sensitive to its steel material type or sizing. However, the conduit temperature is significantly affected by the percentage of surface area that is exposed to heating. A conservative correlation is developed to calculate the internal conduit temperature as a function of the incident heat flux and surface area exposure percentage.

- The peak total heat flux imparted by the fully developed fire at every tunnel location is associated with a time history per Ingason's quadratic design curve for tunnel fires (Ingason 2009). The sensitivity of the curve parameters to total fuel load, growth rate, and decay rate were examined. For all vehicle fire scenarios considered in this study, the total duration of thermal exposure does not exceed 2.5 hours. Based on the results, the peak thermal exposure duration for a standard test to determine conduit fire resistance could range from 30 minutes to 2 hours, depending on a user-defined threshold of fire hazard severity.
- Based on the results of parametric analyses, the thermal impact on exposed electrical conduit can be quantifiably reduced by (1) implementing longitudinal ventilation at critical velocity, (2) reducing the exposure surface area, and (3) relocating the installed location from the ceiling to the sidewall.
- The proposed performance-based approach can enable the selection of tunnel conduit thermal performance criteria as a function of tunnel geometry, ventilation conditions, conduit configuration, and tunnel traffic composition. Due to the importance of continued operation of a tunnel's electrical systems during an emergency, the thermal performance rating for these conduits can be determined as risk tolerance based on expected fire intensity rather than via simple prescriptive thresholds.
- For the conduit considered in this study, performance-based evaluation based on traffic data provided by PennDOT indicated that the following exposure thresholds could be used to develop risk-based fire resistance ratings for conduits that run along the circular tunnel's top-of-ceiling and are fully exposed to fire:
    - To withstand a 50-yr return period fire, the conduit and its contents should remain functional after 2 hrs of exposure to 1095°C (consistent with the mean prescribed value in ASTM E1529) if the tunnel has longitudinal ventilation at critical velocity. Similarly, an exposure temperature of 1500°C would apply for natural ventilation conditions.
    - For a 20-yr return period fire, the corresponding temperature demands decrease to 1150°C and 900°C for the natural and longitudinally ventilated cases, respectively.

CHAPTER 2 – PERFORMANCE-BASED OPTIMIZATION OF STRUCTURAL FIRE MITIGATION STRATEGIES FOR ROADWAY TUNNELS

2.1 Introduction

Vehicle fire hazards pose considerable threats to tunnel structural safety and can lead to long closures for repair. Losing the functionality of the tunnel is always accompanied by huge economic loss including the investment necessary for tunnel repair, the economic impact of traffic detours and accompanied increase in driving time, and associated damage to alternate roadways which may have been designed for a much lower equivalent single axle loads (ESAL). For instance, the Heavy Goods Vehicle (HGV) fire in the Channel Tunnel in 2008 caused a two-day closure and limited service during the four-month repair; resulting in an estimated lost revenue of £185 million ($260 million in 2008) (Wikipedia 2021); the closure of Konigshainer Berge tunnel (Germany 2013) caused damage amounting to €6 million on alternative routes not designed for HGV and a tunnel repair cost of approximately €2.2 million ($2.7 million). Considering the factors of tunnel fire vulnerability due to its enclosed geometry and the bottleneck role in many transportation networks, tunnel fire protection should be carefully considered in the design process.

As stated in NFPA 502 (NFPA 2017), the fire protection method used in the design of the tunnel should account for life safety and ensure: support firefighter accessibility, minimal economic impact, and minimal structural damage. To control the fire impact magnitude or increase the fire resistance of the tunnel structure an active or passive fire protection strategy can be implemented, respectively. Possible active fire protection approaches include: (1) a fire detection system to inform on the occurrence of a fire event; (2) a tunnel ventilation system to facilitate smoke control and temperature reduction; and (3) Fixed Fire-Fighting System (FFFS) to reduce the fire thermal impact and provide fire suppression. Passive fire protection approaches include: (1) a secondary layer of concrete or cementitious material applied to the exposed interior surface of the tunnel; (2) protective material fixed to the tunnel walls and ceiling; and (3) addition of fibers to the main concrete mix to enhance the fire resistance of the concrete. Detailed protection plans may include one approach or a combination of the active and passive fire protection methods. Without making concessions on life safety, the fire protection should be determined based on the specific conditions of the tunnel such as the tunnel dimension (e.g., the cross-section correlates to the tunnel fire vulnerability and the tunnel length directly influences the total investment), the importance of the tunnel in the transportation network (e.g., if the tunnel closure largely increases the cost of traveling or creates increases in traffic); and the budget.

This study proposes a streamlined methodology to optimize the tunnel fire protection approach based on the objectives of minimizing the total protection cost and maximizing the protection efficiency. It could assist the decision-making process on the tunnel fire protection design. With the flowchart presented in Figure 17, the procedure includes three main steps: (1) concrete liner damage assessment considering the passive protection; (2) quantification of the cost associated with implementation of the tunnel fire protection and the corresponding economic loss in the service lifetime due to vehicle fire hazards; and (3) two-objective optimization. In the first step, the typical passive fire protection materials are introduced to MATLAB-SAFIR(Franssen and Gernay 2016) interactive finite element analysis to simulate the concrete spalling behavior and quantify its fire mitigation effect on the concrete liner. The uncertainties associated with the thermal properties of the concrete liner and the protection material are considered with Monte Carlo Simulation. In the second step, for a specific tunnel fire protection plan, the investment and expected economic total loss including the repairment cost and tunnel closure related loss are calculated as the bases for the optimization process in step 3. The tunnel closure time is determined by quantifying the entire damage of the concrete liner using the damage assessment tool in step 1 accompanied with the Confined Discretized Solid Flame (CDSF) model (Guo et al. 2019; Zhu et al. 2022) developed for tunnel fire thermal impact calculation. The tunnel closure-related loss includes the portion resulting from traffic detours and traffic congestion. In step 3, a genetic algorithm is applied to perform the multi-objective optimization to minimize the investment and maximize the protection efficiency. With the generated Pareto front(Wikipedia contributors n.d.), the optimal protection plan(s) provides recommendations for the decision-making process. The approach is based on the authors' best engineering knowledge and publicly available data. With more detailed data or specific information provided by the owner (i.e., the tunnel traffic data, recommended repair procedure and typical repair time, and tunnel detour lengths for the site), this methodology could be adjusted to provide more accurate evaluations.

2.2 Framework and methodology

The process of performing the tunnel fire protection optimization is shown in Figure 17. The three general steps framed with grey dash boxes are labeled as *Step 1*: develop correlation between damage level, heat flux and exposure duration for protection scheme and concrete tunnel construction details; *Step 2*: calculate the cost of potential tunnel fire protection schemes and determine the corresponding expected economic loss in tunnel service over operation lifetime; and *Step 3*: multi-objective optimization based on potential constraints in cost, operation, and life safety. Each of these three steps can be conducted separately, which allows for independent parameter generation using Monte Carlo Simulation. For example, the concrete thermal properties directly impact the amount of tunnel liner damage in step 1, but are independent of the thermal impact and the traffic-related economic loss evaluations conducted in step 2.

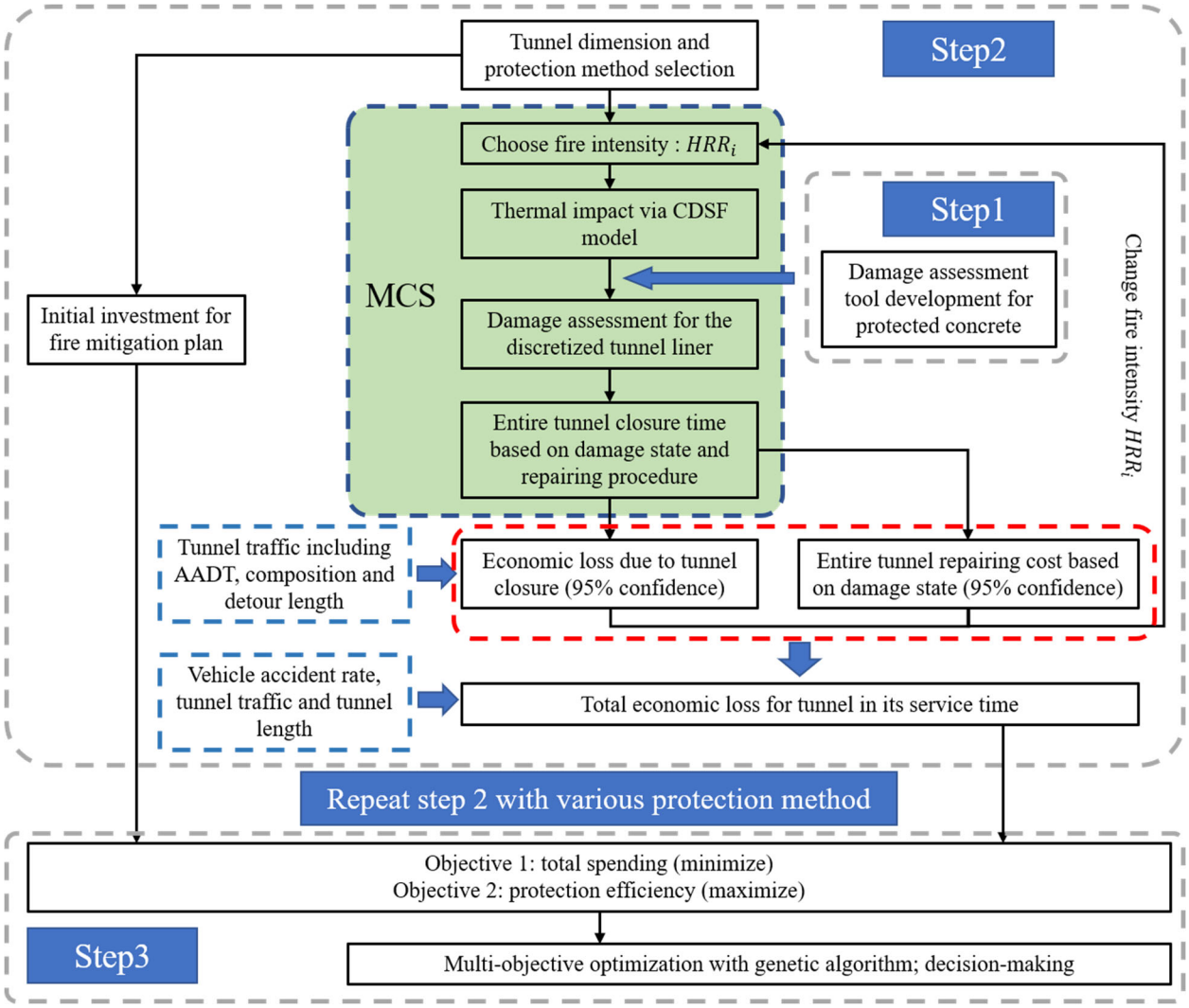

Figure 17: Flowchart of tunnel fire protection optimization

2.2.1. Damage assessment for the concrete liner with passive fire protection

During a fire event the tunnel concrete liner could experience permanent material strength reduction due to dehydration of the chemically bound water from the concrete and explosive spalling due to rapid movement of moisture and elevated pore pressures in the section (Beard and Carvel 2005). These effects impact the integrity of the structural cross-section and can expose the deeper concrete material and steel reinforcement to direct heat exposure resulting in progressively increasing damage to the section. To provide enhanced performance under a fire event passive fire protection can be utilized. This section focuses on the most commonly used options: fire protection material attached to the concrete surface including the spray-applied fire-resistive material (SFRM)(Isolatek International n.d.) and Calcium-silicate based fire protection board (*fermacell AESTUVER Fire safety concepts for underground transport systems* n.d.; Promat n.d.). These protection approaches are required to be durable (e.g., fire protection boards are required to have a service life of at least 25 years (Leucker n.d.)); are easily applied to circular or horseshoe

tunnels; have been tested to the latest industry fire standards (RWS, hydrocarbon, and jet fire); and are easily repaired if damaged. The CAFCO ® FENDOLITE M-II/ ISOLATEK® Type M-II SFRM and the fire protection board PROMATECT® -H, PROMATECT® -T, PROMATECT®-TFX, and AESTUVER®-T have been widely used in tunnel fire protection in the past few decades. Fire protection boards act as a barrier to mitigate the heat penetration with their low thermal heat conductivity. The thickness of the protection product can be optimized to provide the most efficient solution based on the expected demands in the tunnel. This study utilizes the publicly available data of these protection materials and investigates the mitigation performance under thermal demands. The uncertainties of thermal properties of both the passive fire protection material (including both SFRM and fire protection board) and the concrete liner are considered with Monte Carlo Simulation (MCS). The models used are developed in the next section.

2.2.1.1. Thermal properties of passive fire protection and concrete

The thermal properties of SFRM was experimentally assessed by Kodur and Shakya (2013) (Kodur and Shakya 2013) and the National Institute of Standards and Technology (NIST) (2005) (Nicholas Carino et al. 2005). Properties of these insulation materials vary based on the product. Since no technical data is provided by manufacturers for the SFRMs specially applied to tunnels, the stochastic properties of SFRM are based on past research on building applications. Accounting for the uncertainties, Negar et al. (2015) (Khorasani et al. 2015) proposed the probabilistic model of the density ρ_i (kg/m^3), thermal conductivity k_i (W/m·K) and specific c_i (J/kg·K) heat for a typical SFRM based on the measured data by NIST (Khorasani et al. 2015) as expressed with Eq. (15) to (17) respectively:

$$\rho_i^{SFRM} = \exp(-2.028 + 7.83 \times T^{-0.0065} + 0.122 \times \varepsilon) \quad (15)$$

$$k_i^{SFRM} = \exp(-2.72 + 1.89 \times 10^{-3} \times T - 0.195 \times 10^{-6} \times T^2 + 0.209 \times \varepsilon) \quad (16)$$

$$c_i^{SFRM} = 1{,}700 - \exp(6.81 - 1.61 \times 10^{-3} \times T + 0.44 \times 10^{-6} \times T^2 + 0.213 \times \varepsilon) \quad (17)$$

where T is the temperature in degrees Celsius and ε is a random variable in accordance with the standard normal distribution. The thermal conductivity and specific heat, which are sensitive to the concrete thermal behavior, are presented with dash curves in Figure 18. To optimize the SFRM application, the thickness of the material is assumed to vary from thin to thick with an increment of 6.35mm (0.25in).

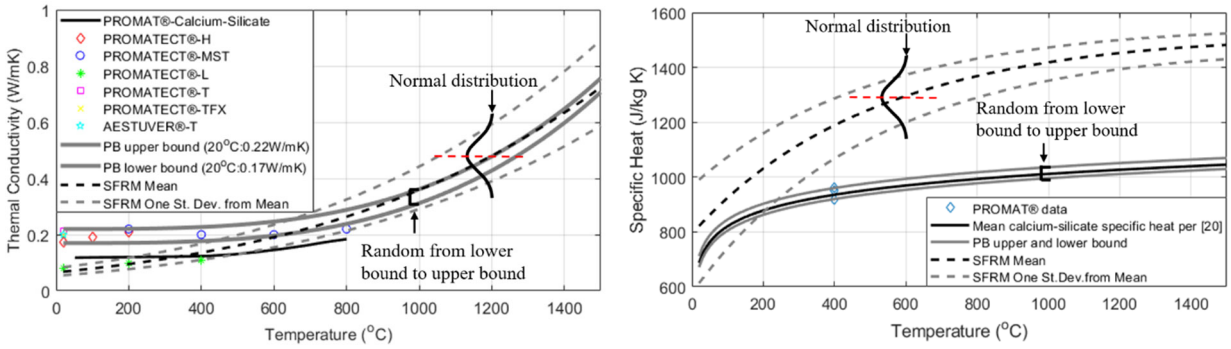

(a) Thermal conductivity (b) Specific heat

Figure 18: Thermal properties of the protection board and SFRM

The thermal properties of the fire protection board such as Promat ® and AESTUVER ® are based on manufacturers data (AESTUVER n.d.; Promat International n.d., n.d., n.d.). Table 7 lists the thermal properties of PROMATECT®-T, PROMATECT®-H PROMATECT®-TFX and AESTUVER®-T which were specially developed for tunnel fire protection along with PROMATECT®-L and PROMATECT®-MST which was developed for other applications such as industry furnaces protection to complement data for temperature-dependent expression development. The data is presented as a scatter plot in Figure 18.

Table 7: Thermal material of the fire protection board

Brand	Material type	Thermal conductivity (W/m-K) (ASTM C518-75)	Moisture content	Thickness (mm)	Specific heat (kJ/kg K)	Density (kg/m^3)
Board applied to the tunnel						
PROMATECT® -H (RWS/HCM)	Calcium-silicate based	0.175-0.19-0.21 (20°C-100°C -200°C)	5-10%	6-25mm	0.92 (400°C)	870
PROMATECT® -T	Calcium-silicate based	0.212 (20°C)	5%	15-40mm	N/A	900
PROMATECT® -TFX	latest (Matrix Engineered Mineral Board)	0.20 (20°C)	5%	20-40mm	N/A	950
AESTUVER®-T	Calcium-silicate based	0.175 (20°C)	N/A	N/A	N/A	690-980
Board of other applications (e.g. industry furnaces, dryers)						
PROMATECT® -L	Calcium-silicate based	0.08-0.10-0.11 (20°C-200°C -400°C)	N/A	20-50mm	0.96 (400°C)	N/A
PROMATECT® -MST	Calcium-silicate based	0.22-0.20-0.20-0.22 (200°C-400°C -600°C -800°C)	5%	12-60mm	0.95 (400°C)	N/A

Calcium-silicate fire protection board provides stable thermal properties throughout a wide range of temperatures. Calibrated with the data for tunnel fire protection board in The thermal properties of the fire protection board such as Promat ® and AESTUVER ® are based on manufacturers data (AESTUVER n.d.; Promat International n.d., n.d., n.d.). Table 7 lists the thermal properties of PROMATECT®-T,

PROMATECT®-H PROMATECT®-TFX and AESTUVER®-T which were specially developed for tunnel fire protection along with PROMATECT®-L and PROMATECT®-MST which was developed for other applications such as industry furnaces protection to complement data for temperature-dependent expression development. The data is presented as a scatter plot in Figure 18.

Table 7, the temperature-dependent thermal conductivity and specific heat expressions (as in Eq. 18 and Eq. 19 respectively) are developed following the format for typical calcium-silicate material in the Promat technical brochure (Promat 2014), and the study by Ohmura et al. (2003) (Ohmura et al. n.d.) based on experiments, respectively.

$$k_i^{PB} = 2.035 \times 10^{-11} \times T^{3.281} + 0.17 + 0.05 \times \alpha \tag{18}$$

$$c_i^{PB} = 4.23 \times 10^{-1} + 8.29 \times 10^{-2} \times \ln(T) + 0.04 \times \alpha \tag{19}$$

where α is randomly chosen from 0 to 1 to create a parallel shift in the base curves allowing for an envelope of the measured data. The curves along with the data are shown in Figure 18 with solid gray curves. The density of the protection board at ambient temperature, ρ_{20}^{PB}, is deterministically taken as 890 kg/m^3, the mean value of the listed data in The thermal properties of the fire protection board such as Promat ® and AESTUVER ® are based on manufacturers data (AESTUVER n.d.; Promat International n.d., n.d., n.d.). Table 7 lists the thermal properties of PROMATECT®-T, PROMATECT®-H PROMATECT®-TFX and AESTUVER®-T which were specially developed for tunnel fire protection along with PROMATECT®-L and PROMATECT®-MST which was developed for other applications such as industry furnaces protection to complement data for temperature-dependent expression development. The data is presented as a scatter plot in Figure 18.

Table 7. The variation of the density with elevated temperature is considered to follow the equation for concrete in Eurocode 1 (CEN 2008).

The thermal properties of concrete liner are based on stochastic models proposed by Jovanović, B., et al. (Jovanović et al. 2020) with mean and standard deviation for temperature-dependent thermal capacities and specific heat expressed in Eq. (20) and (21) respectively. The concrete thermal conductivity and specific heat for a given temperature are assumed to follow a Gamma distribution.

$$k_{i\_mean}^{conc} = 6.627 \times 10^{-7} \times T^2 - 1.458 \times 10^{-3} \times T + 1.772 \tag{20a}$$

$$k_{i\_std}^{conc} = 3.139 \times 10^{-7} \times T^2 - 0.691 \times 10^{-3} \times T + 0.434 \tag{20b}$$

$$c_{i\_mean}^{conc} = -2.953 \times 10^{-7} \times T^2 - 6.498 \times 10^{-4} \times T + 0.872 \tag{21a}$$

$$c_{i\_std}^{conc} = -3.500 \times 10^{-7} \times T^2 - 7.700 \times 10^{-4} \times T + 0.042 \tag{21b}$$

The specific heat variation with temperature is modified to account for the increase that occurs above 100°C due to the removal of free water from the concrete matrix. The modification follows recommendations of Eurocode 2, and varies with moisture content. It consists of a plateau between 100°C and 115°C, and linearly decreases between 115°C and 200°C to the equation 21 curve. Details on this modification are outlined in the tunnel resilience study in the report of Year 3 Task 2.

2.2.1.2. Concrete liner thermal analysis and damage classification

The performance of the concrete liner subjected to thermal impact is simulated with a MATLAB-SAFIR interactive finite element analysis that accounts for fire induced spalling. Shown in Figure 19, the 2D model for thermal finite element analysis in SAFIR is constructed according to the scheme of the protected concrete liner. The thickness of the concrete cover is defined at 50mm (2in.) (Commonwealth of Pennsylvania 2016) while the cross-section thickness of the liner is assumed to be 0.3m (11.8in) (Guo et al. 2019). The reinforcement was represented as a thin smeared layer, as opposed to individual circular cross-sections, and was located behind the concrete cover. The cover was discretized into 20 fiber elements (in 2.5 mm thick layers) to accurately simulate spall behavior depths. A thin concrete layer is placed 19 mm (0.75 in.) behind the steel reinforcement layer to assess if the temperature at the removal thickness is thermally compromised for the "Heavy" damaged concrete liner as stated in the damage classification discerption follows. The remaining concrete liner is meshed at 12.7 mm (0.5 in.) per layer to capture the thermal penetration and help quantify the thickness of unsounded concrete that requires further removal. The passive fire protection attached to the concrete cover is meshed into 10 fibers and indicated with blue color is in Figure 19.

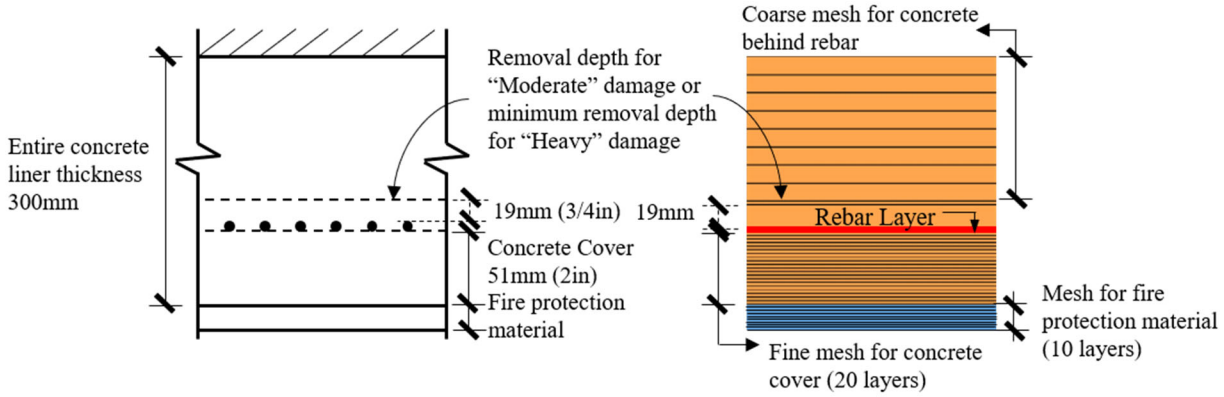

Figure 19: Prototype concrete tunnel liner geometry and fiber model

The spalling behavior of the concrete liner, which is commonly observed in both practical fire hazards and experiments, is modeled with MATLAB-SAFIR interactive finite element method with the process explained and framed with the blue dash box in the flowchart presented in Figure 20. Generally, a portion of the concrete cover reaching the predefined threshold of spalling (i.e., concrete surface temperature

reaching 740°C) is removed from the finite element model, exposing the new surface frontier to the thermal impact. The spalling depth is determined based on the experiments by Lu (2015) (Lu 2015), which indicates the range of material temperatures at the spalling depth is between 250°C and 400°C. Therefore, the concrete spalling is assumed to occur from the triggering surface temperature of 740°C to the internal layer which is at 250°C. The newly formed concrete liner model inherits the temperature distribution of the previous step and continues the spalling simulation for the new iteration. The spalling stops either when the exposure time is reached or the reinforcement layer is exposed. To note, the protection material is removed from the finite element model for the concrete liner in the first iteration of spalling both for the case of the SFRM and the protection board for conservatism. In this process of thermal analysis, the convective coefficients for the fire-exposed and unexposed surfaces were 25 W/m^2-K and 9 W/m^2-K, respectively, per Eurocode 1, Part 1-5 (CEN 2002). The emissivity of concrete was defined at 0.7 per Eurocode 2 (European Committee for Standardization 2004).

The damage state of the concrete liner is categorized into three classes from superficial to heavy according to the post-fire repair procedure required. The criteria for each damage level are indicated in Figure 20 and described as follows:

- **Superficial**: The temperature of the heated surface was below 300°C. The concrete surface color remains unchanged. The residual strength is consistent with the value prior to the fire. No repair is required structurally for this level of damage.
- **Moderate**: The concrete experienced a temperature higher than 300°C and the surface may spall during the heating process however, the estimated spall depth is shallower than the concrete cover. For this damage level, the strength of concrete is permanently reduced as aforementioned. The unexposed reinforcement is considered intact as the remaining concrete cover provides adequate thermal insulation and constraint. Repair consists of removal of the deteriorated concrete to a depth of 19 mm behind the reinforcement, which is presented in Figure 20, and replacement with shotcrete. The repair process requires full tunnel closure.
- **Heavy**: The concrete has spalled to the depth of the reinforcement. During the event, the exposed reinforcement has experienced temperatures exceeding 600°C resulting in permanent yield strength reduction (Ingham 2009). The compromised reinforcement should be removed and replaced. Concrete should be removed to a depth of 19 mm behind the reinforcement. Unsound concrete will likely be present beyond this point and further removal should be performed with the permission of the responsible structural engineer to ensure that the global structural integrity is not compromised (indicated in Figure 20). The repair process requires full tunnel closure.

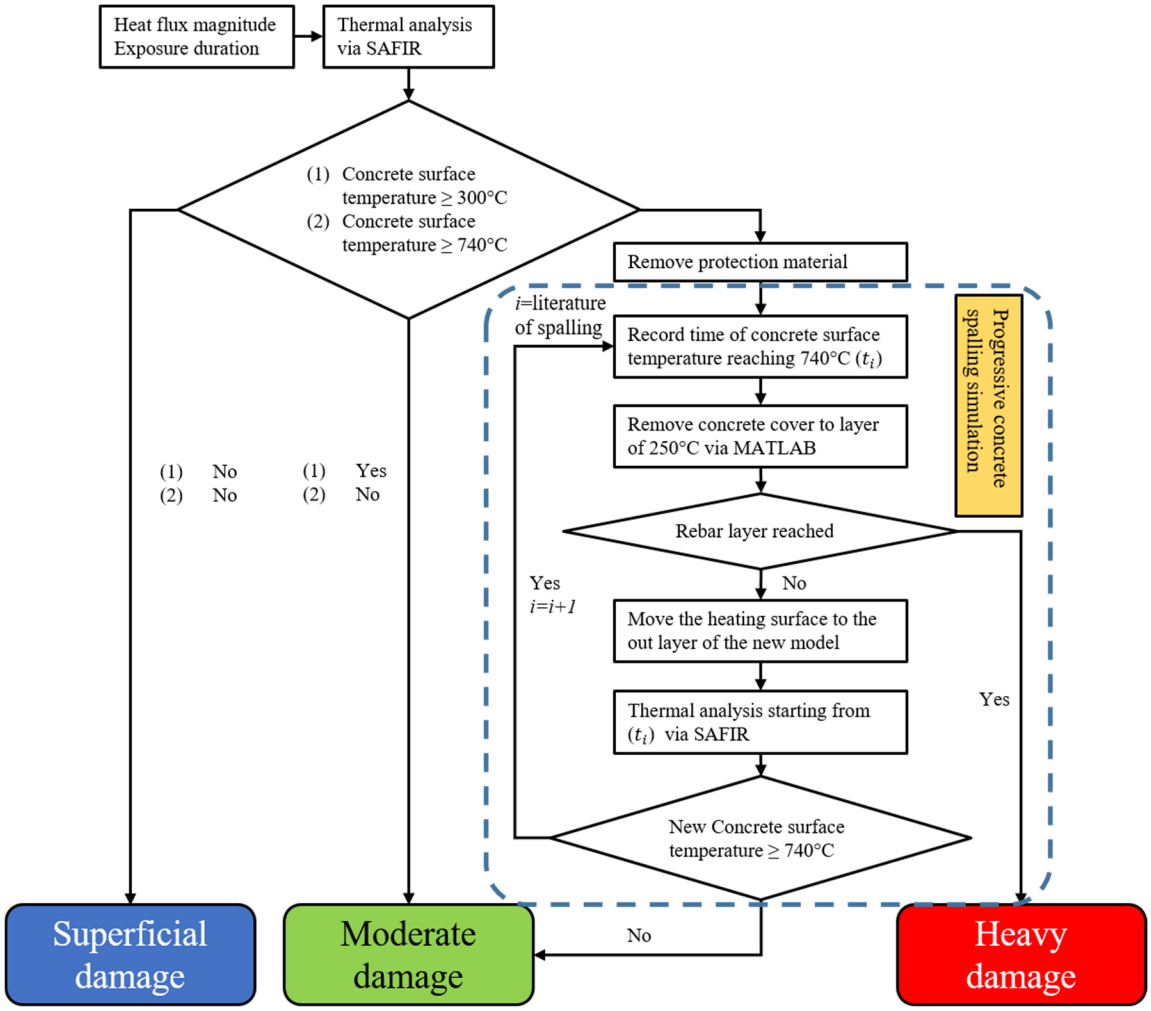

Figure 20: Flowchart of thermal analysis and damage classification for concrete liner

2.2.1.3. Stochastic analysis

The damage assessment tool for the protected concrete liner is developed via Monte Carlo Simulation (MCS) with Latin hypercube sampling (sample size of 2,000), considering the uncertainties associated with the thermal properties of both concrete and protection materials. The input parameters with their corresponding distributions are summarized in Table 8. The thermal impact, which is expressed with the heat flux magnitude and exposure duration, is randomly selected between the predefined lower bound and upper bound.

Table 8: Input parameters for protected concrete damage assessment tool development

SFRM					
Description	Unit	Distribution	Value of parameters		Temperature dependent equation
Density ρ_i^{SFRM}	kg/m^3	Normal	$\varepsilon_{mean} = 0$	$\varepsilon_{std} = 1$	Eq. (15)
Conductivity k_i^{SFRM}	W/m^2·K	Normal	$\varepsilon_{mean} = 0$	$\varepsilon_{std} = 1$	Eq. (16)
Specific heat c_i^{SFRM}	J/kg· K	Normal	$\varepsilon_{mean} = 0$	$\varepsilon_{std} = 1$	Eq. (17)
Protection board					
Density ρ_i^{PB}	kg/m^3	Deterministic	890 kg/m^3		Eq. (20)
Conductivity k_i^{PB}	W/m^2·K	Uniform	$\alpha_{lower} = 0$	$\alpha_{upper} = 1$	Eq. (18)
Specific heat c_i^{PB}	kJ/kg· K	Uniform	$\alpha_{lower} = 0$	$\alpha_{upper} = 1$	Eq. (19)
Concrete thermal properties					
Density ρ_i^{conc}	kg/m^3	Normal	$\rho_{i\ mean}^{conc}$ =2350 kg/m^3	$\rho_{i\ std}^{conc}$ =16.7 kg/m^3	Eq. (20)
Conductivity k_i^{conc}	W/m^2·K	Gamma	$k_{i\_mean}^{conc}$ via Eq. (21)	$k_{i\_\mathrm{std}}^{conc}$ via Eq. (21)	Eq. (21)
Specific heat c_i^{conc} (u=0.0 %)	kJ/kg· K	Gamma	$c_{i\_mean}^{conc}$ via Eq. (22)	$c_{i\_\mathrm{std}}^{conc}$ via Eq. (22)	Eq. (22)
Moisture content u	-	Gaussian	u_{mean}=4.46%	u_{std}=0.2%	N/A
Fire exposure parameters					
Heat Flux $\dot{q}$	kW/m^2	Uniform	$\dot{q}_{lower}$ =50	$\dot{q}_{upper}$ =400	N/A
Exposure duration t	min	Uniform	t_{lower}=0	t_{upper} =120	N/A

A stochastic thermal analysis of the prototype tunnel liner geometry (Figure 19) with three passive fire protection approaches (e.g., 8mm and 15 mm fire protection board of 8mm, 15mm or 12.7 mm SFRM) is illustrated. Each simulated case is categorized into the pre-defined damage classes based on the performance under the stochastic event. Figure 21a, Figure 22a, and Figure 23a present the full result set for the 2,000 randomized simulations with the damage level indicated with different colors for each of the three cases. As expected, when thicker fire protection is used, a higher heat flux magnitude and longer exposure time are required to reach higher damage levels.

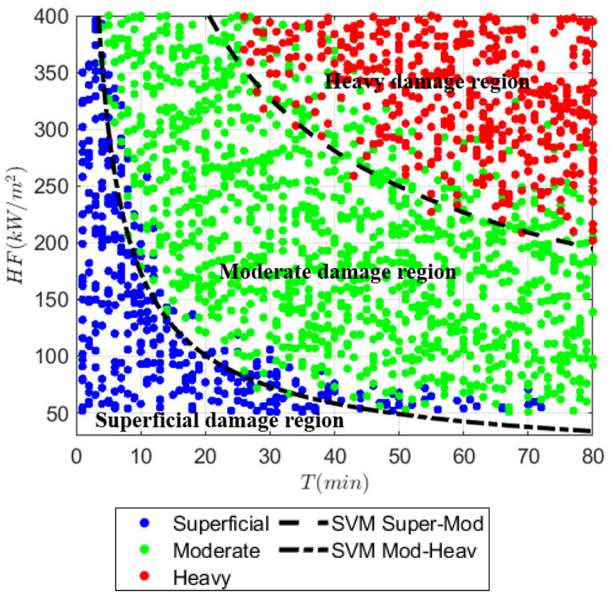

(a) Thermal impact expressed with heat flux and exposure duration

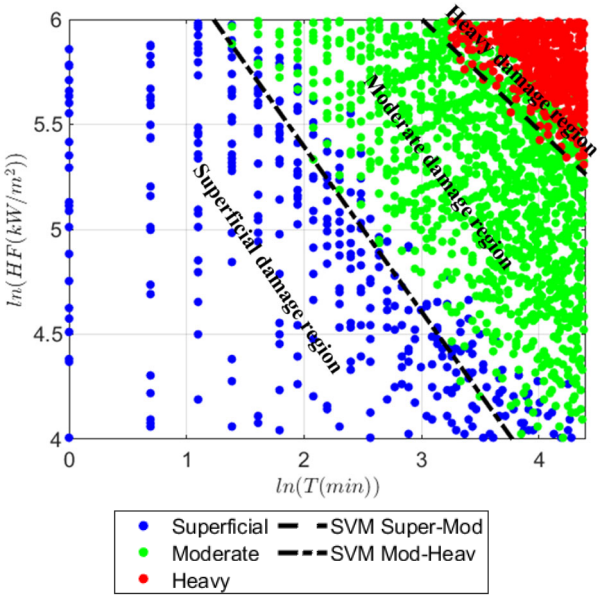

(b) Thermal impact expressed with ln (heat flux) and ln (exposure duration)

Figure 21: Damage classification tool for concrete panel with fire protection board of 8mm

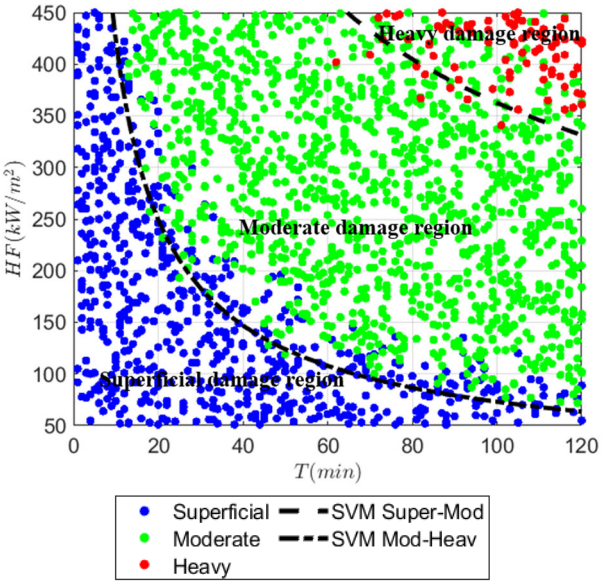

(a) Thermal impact expressed with heat flux and exposure duration

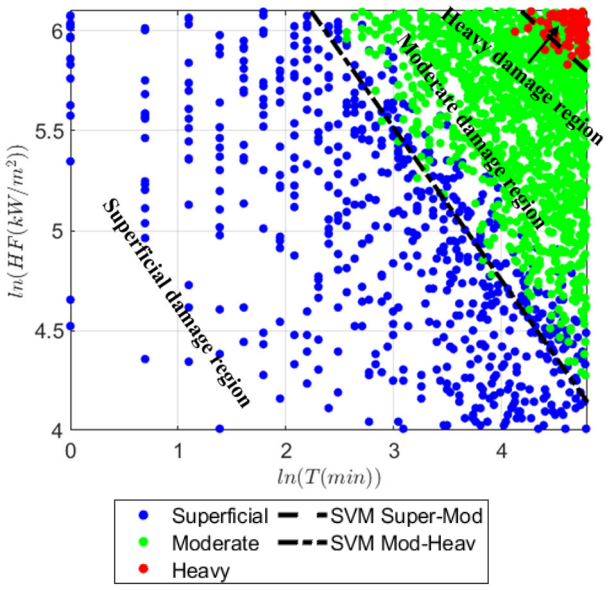

(b) Thermal impact expressed with ln (heat flux) and ln (exposure duration)

Figure 22: Damage classification tool for concrete panel with fire protection board of 15mm

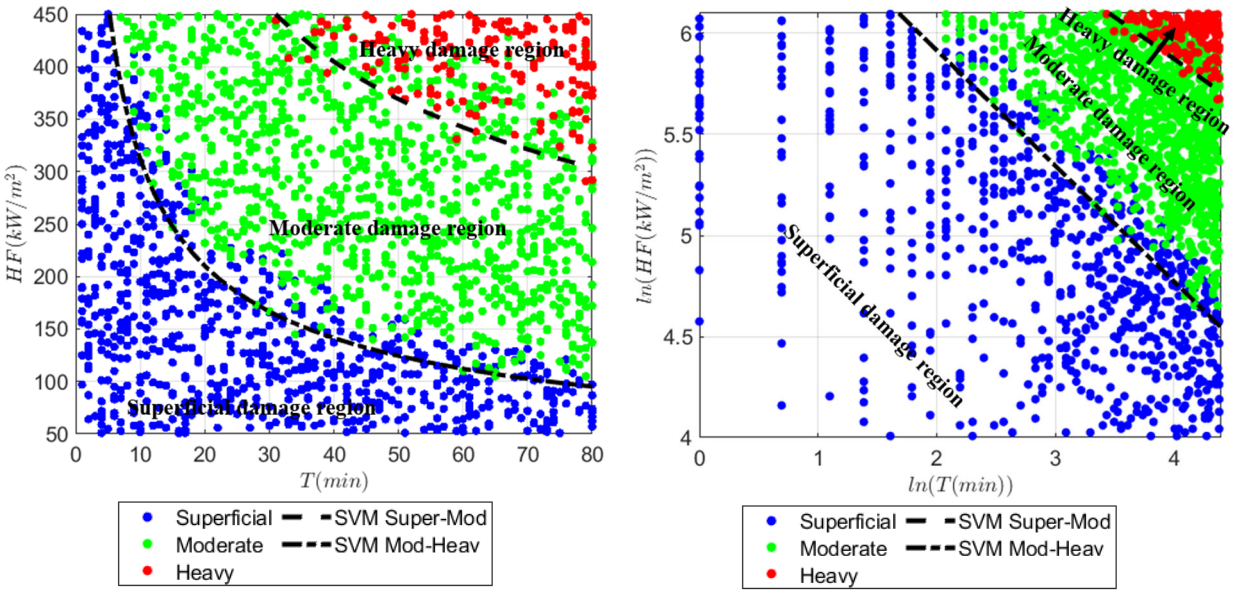

(a) Thermal impact expressed with heat flux and exposure duration

(b) Thermal impact expressed with ln (heat flux) and ln (exposure duration)

Figure 23: Damage classification tool for concrete panel with SFRM of 12.7mm (0.5in)

As illustrated in the stochastic results, boundaries are present from one damage level to another. These precomputed divisions can be defined and used to classify the expected damage without the need to repeat the finite element thermal analyses. Due to the stochastic analysis approach, the damage conditions overlap at the boundary. To define a single division between the damage states the natural logarithm of the results are taken (Figure 21 through Figure 23 (a) to (b)). These results are then evaluated using a supervised machine learning approach, the Support Vector Machine (SVM) classifier with linear kernel function (Cortes and Vapnik 1995). Generally, this algorithm searches for an optimal hyperplane that separates the data into two classes. For the case of inseparable data, this algorithm imposes a penalty on the length of the margin for each observation located on the wrong side. To provide a conservative estimation of the damage state (i.e., rarely classify the heavy damage case as moderate damage), the misclassification cost matrix is set to be $\begin{bmatrix} 1 & 0 \\ 0 & 5 \end{bmatrix}$, which amplifies the penalty of the margin-violation observations of the higher damage classes by 5 times. Shown in (b) series in Figure 21 through Figure 23, the developed liner boundaries, which are plotted with black dashed lines, effectively delineate the concrete liner damage regions while allowing only a few observations to escape to the lower damage level. The liner binary classification is performed with the built-in MATLAB function and expressed with Eq. (22).

$$w_1 \cdot \ln(\dot{q}) + w_2 \cdot \ln(t) + b = 0 \tag{22}$$

where w_1 and w_2 are weighting factors and b is the bias term. Transferring these linear boundaries to the normal scale space, the non-linear boundaries resemble the shape of Pressure-Impulse (P-I) curves,

commonly used blast resistant building design (U.S. Army Corps of Engineers 2008), as presented in (a) series of Figure 21 through Figure 23. The stochastic analysis and damage boundary determination is repeated for five additional protection cases, resulting in two SFRM thicknesses, five protection board thicknesses and an unprotected case. Table 9 summarizes the associated parameters to allocate these boundaries for each case.

Table 9: Parameters for damage classification boundaries for specific passive fire protection

	Parameters	Passive fire protection plan						
		No Protection	SRFM: 12.7 mm	PB: 8mm	PB: 12mm	PB: 15mm	PB: 18mm	PB: 20mm
Damage classification								
Superficial - Moderate	w1	1.852	3.05	2.91	3.12	3.22	3.52	3.53
	w2	3.953	5.33	3.71	4.22	4.21	4.50	4.56
	b	-18.39	-37.64	-25.83	-31.18	-32.88	-36.81	-37.98
	Slope	-0.47	-0.57	-0.78	-0.74	-0.76	-0.78	-0.77
Moderate-Heavy	w1	3.609	3.24	3.66	3.44	3.74	N/A*	N/A
	w2	6.924	7.84	6.91	7.38	7.58	N/A	N/A
	b	-45.11	-59.02	-52.47	-57.31	-61.90	N/A	N/A
	Slope	-0.52	-0.41	-0.53	-0.47	-0.49	N/A	N/A
Depth of further removal								
$d_{removal}$ (95%)-m	p1	0.025	0.0407	0.0394	0.0429	0.0516	N/A	N/A
	p2	0.024	0.0658	0.0578	0.0552	0.0591	N/A	N/A
	p0	-0.1864	-0.534	-0.461	-0.477	-0.673	N/A	N/A

*Note: value is not provided since the heavy damage case is not observed in the simulated cases.

For concrete liner classified with heavy damage, the concrete 19 mm (¾ in.) past the reinforcement layer may experience a temperature exceeding 300°C, which indicates significant concrete material damage (Bergeson and Ernst 2015; Ingham 2009; Joint ACI/TMS Committee 216 and Masonry Society (U.S.) 2007). This portion of the concrete must be removed and replaced during repair. The additional removal depth for the heavy damage class can be determined as a function of the heat flux and exposure time for each protection approach. A regression plane is introduced to fit the further removal depth starting from 19mm (¾ in) behind the reinforcement (referring to Figure 19) in the *ln-ln* space defined by heat flux magnitude and exposure duration. As presented in Figure 24 for the case of the 8mm protection board, the heavy damage cases are clustered in five vertical planes with each plane corresponding to the fiber discretization. The blue surface represents the mean regression of the data set. To provide a confidence on the plane, the surface is moved in a parallel shift until the 95% of the data points are encompassed, the

green plane expressed with Eq. (23) is developed to provide a conservative estimation of the further concrete removal depth.

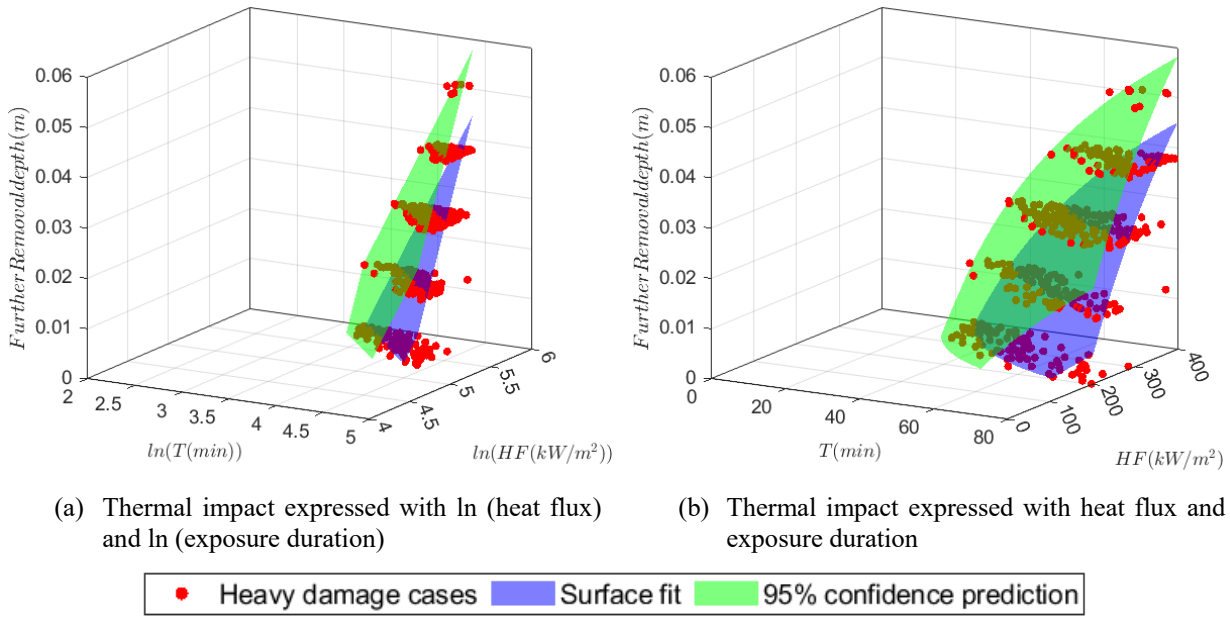

(a) Thermal impact expressed with ln (heat flux) and ln (exposure duration)

(b) Thermal impact expressed with heat flux and exposure duration

Figure 24: Further concrete removal depth of heavy damaged class and surface regression for prediction

$$d_{removal}(95\%) = p_1 \cdot \ln(\dot{q}) + p_2 \cdot \ln(t) + p_0 \tag{23}$$

where the non-dimensional coefficients p_1, p_2 and the bias term p_0 varies with the selected passive fire protection plan and is listed in Table 9.

The damage classification maps together with the equations to determine additional concrete removal for the heavy damage cases provides the damage assessment tools needed for unprotected and the passive protected prototype concrete liner. Given specific thermal input expressed as heat flux magnitude and exposure duration, the damage state can be easily estimated. This allows for the quantification of repair required and the associated tunnel closure time. In this study, the two passive fire protection methods are investigated on the prototype concrete liner geometry for illustration purposes. This approach can be extended to other passive protection schemes and concrete liner reinforcement strategies given the necessary information on material thermal properties and associated uncertainties.

2.2.2. Protection Investment

The implementation of a tunnel fire protection plan is always accompanied by a large financial investment. This includes not only the initial construction cost but also the operation and maintenance costs over the tunnel service lifetime. Table 10 lists the publicly available cost information on the use of protection boards, FFFS, and longitudinal ventilation fire protection plans. For the tunnel fire protection board, the insulationshop.co website (Insulationshop.co n.d.) provides the price of the Promat® fire

protection board with the size of 2440mm × 1220mm and thickness ranging from 6mm to 20mm. The unit price for the protection board of other thicknesses (i.e., 8mm and 15mm) can be interpolated from the available data. The cost data for FFFS and their annual maintenance cost varies greatly, as noted in Table 10. This study relies on the data provided in the STUVA Conference 2011 at Berlin (Dipl.-Ing and Dipl.-Ing. n.d.) in the case study in section 2.3. A sensitivity analysis is performed to study the influence of the cost in section 2.4. The tunnel ventilation design depends on the dimension of the tunnel (i.e., tunnel height, tunnel cross-section area, and shape; tunnel length; the number of lanes and tunnel gradient), design fire hazard intensity and location, and the power of the selected jet fans. Mosen Ltd.(Mosen Ltd 2022), which is a company expertized in tunnel fire safety engineering, provides an excel sheet allowing a preliminary tunnel ventilation calculation and estimation of the required number of jet fans that should be installed for specific tunnel conditions. Moreover, the net present cost is then calculated also via the excel sheet provided by Mosen, considering the annual installed power cost, installation cost, procurement cost, and yearly maintenance cost with the write-off period of 20 years as listed in Table 10. In the life cycle cost calculation process, the current interest rate should be considered while the inflation rate is dropped off for the uniform price change for all payment variables and its large uncertainties. In the United States, the authority to set interest rates is divided between the Board of Governors of the Federal Reserve (Board) and the Federal Open Market Committee (FOMC). According to the UD Federal Reserve Bank, the current interest rate varies from 1.25% to 2.50% from the beginning of 2017 to 2020 and stays stable at 1.75% before the economic impact resulting from COVID-19. This study uses 1.75% as the interest rate for the calculation of life cycle costs. In the tunnel service lifetime, the facilities including the ventilation system, FFFS, and protection board should be replaced several times, which causes re-investment. By summing the cost for each individual fire protection method, the total present investment for a specific protection plan can be calculated. To note, in the case that tunnel liner is protected with SFRM, the information such as the investment, application and removal rate and the maintenance requirement is not adequate on the publicly available literature. Hence, this passive protection method is not included in the subsequent tunnel fire mitigation optimization process illustrated in the case study in section 2.3.

Table 10: Investment for tunnel fire protection methods

Promat fire protection board						
Board thickness (mm)	6		9	12	20	Recourse
Protection board material cost (USD/ m^2)	41.31		65.80	87.26	157.0	insulationshop.co website (Insulationshop.co n.d.)
Protection board installation fee (USD/ m^2)			81.36			
Protection board installation fixed fee (USD)			5,811.7			AESTUVER report (Leucker n.d.)
Maintenance cost (USD/ m^2)			1.74			
Maintenance cycle (years)			6			
Use life (years)			30			
FFFS						
Installation of FFFS system (million USD/km)			0.58-2.35 (mean value of 1.45)			STUVA Conference 2011 at Berlin (Dipl.-Ing and Dipl.-Ing. n.d.)
Maintenance fee			Annually 0.3%-1.25% of the installation fee (mean value of 0.78% applied in this study)			
Use life (years)			30			
Installation of FFFS system (million USD/ km)			3			Jonsson & Johnson (Anurag 2017)
Maintenance fee (million USD/km)			Annually 0.36 (12% of the installation fee)			
Use life (years)			30			
Installation of FFFS system (million USD/km)			2-lane or 3-lane circular tunnel: 3.39			Codot (CoDOT n.d.)
Ventilation system						
Tunnel size			three-lane circular tunnel			Mosen Company (Mosen Ltd 2022)
Tunnel length (m)	≤200	800	1335.6 (Lehigh tunnel)	1600	3200	
No. of jet fans	6	18	22	26	44	
Net present investment for jet fans (million USD)	1.924	5.77	7.05	8.34	14.11	
Use life (years)			20			
Tunnel size			two-lane circular tunnel			
Tunnel length (m)	≤200	800	1335.6 (Lehigh Tunnel)	1600	3200	
No. of jet fans	6	12	16	18	30	
Net present investment for jet fans (million USD)	1.924	3.85	5.13	5.77	9.62	
Use life			20 years			
Tunnel size			two-lane			Codot (CoDOT n.d.)
Tunnel length (m)			2651			
Net investment (million USD)			8.53			
Tunnel size			three-lane			
Tunnel length (m)			2651		1036	
Net investment (million USD)			12.4		4.33	

2.2.3. Tunnel fire impact calculation through CDSF model

The thermal impact results from vehicle fires is calculated via CDSF model, which has been introduced in section 1.3.1. It combines the radiative and convective heat flux received by the tunnel structural elements for both the natural and longitudinal ventilated scenarios. The detailed development and description refer to the report of Year 3 Task 2.

The heat flux time history for each panel is generate by scaling the HRR time history curve, which is proposed by Ingason (Ingason 2009) for tunnel fire design, which is introduced in section 1.3.2. with the magnitude calculated via the CDSF model.

The heat flux time history curve for each panel is then converted to a thermal impact expressed with the constant peak heat flux magnitude ($\dot{q}''_{total,j}$) and exposure time (t_j) based on energy equivalency. It is conservative because the condensed thermal impact results in higher concrete temperatures and corresponding damages. Implementing these two parameters for each discretized concrete liner into the damage assessment map illustrated in Figure 21 through Figure 24 iteratively, the damage state for the entire protected tunnel can be estimated. Figure 25 (b) shows the distribution of the damage of concrete liner protected with the 8mm fire protection board according to the thermal impact presented in Figure 25 (a).

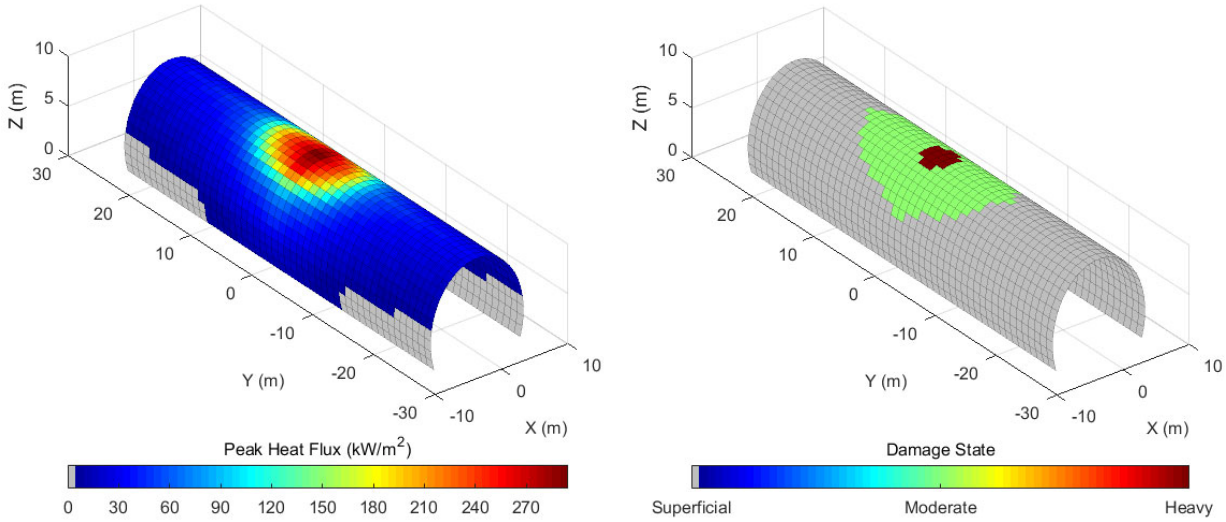

(a) Heat flux distribution (b) Damage state

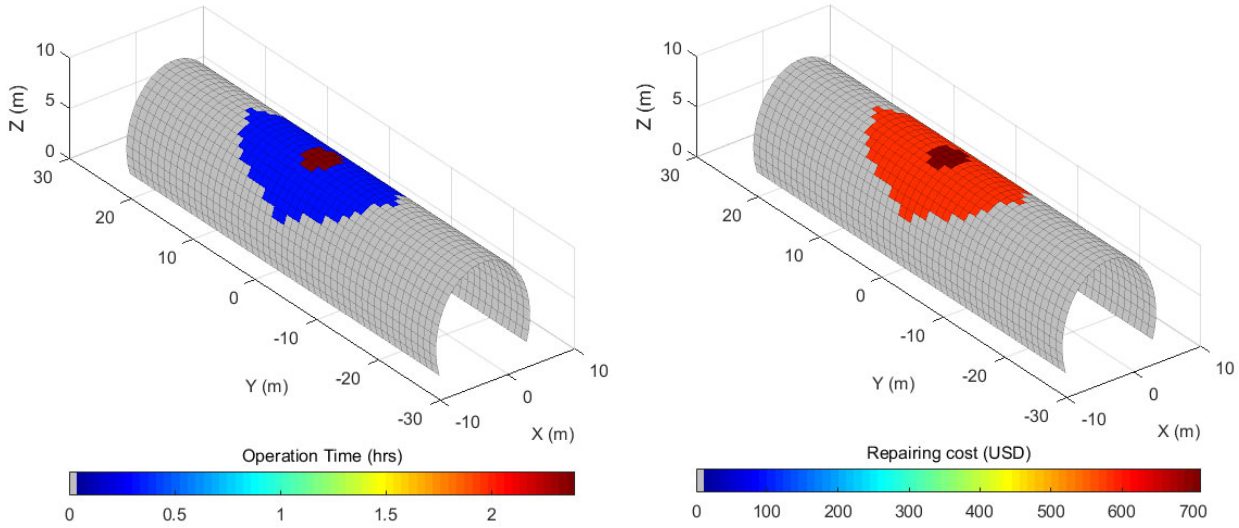

(c) Repairing time (d) Repairing cost

Figure 25: Distribution of (a) heat flux (b) damage state (c) repairing time and (d) repairing cost for the natural ventilated 3-lane circular tunnel with 8mm fire protection board subjected to fire hazard of 200MW

2.2.4. Economic loss due to fire hazard

The economic loss due to tunnel fire hazards consists of the repair cost and the traffic-related loss as shown in Figure 17. Both of these portions correlate to the tunnel damage state, which could be quantified with the calculated thermal impact and damage assessment tool developed in section 2.2.1. It is assumed that the tunnel is entirely closed for the repair procedure, which results in traffic detours and traffic jams during the repair period duration. The tunnel traffic volume and composition are used for both the expected damage assessment and the traffic-related loss calculation.

2.2.4.1. Tunnel closure time for repairment

The post-fire tunnel repair requirements are based on the preceding damage assessment. The concrete tunnel liner can be discretized and the damage level and associated repair requirement for each element can be determined. The overall tunnel closure time can be determined by applying estimated rehabilitation rates as noted in Table 11**Error! Not a valid bookmark self-reference.**. These values are based on authors' engineering judgment as no detailed specifications for tunnel fire repair is available according to a MassDOT (2021) investigation (Gerasimidis and Civjan n.d.).

Table 11: Protected tunnel concrete liner repair procedure post-fire

Procedure	Rate	Damage state			Comments
		Superficial	Moderate	Heavy	
Protection board removal	24 m^2/hr (200 ft^2/hr)	None	✓	✓	Area x 2
Concrete inspection	18.6 m^2/hr (200 ft^2/hr)		✓	✓	
Concrete removal (stage 1)	1.22 m^3/hr (1.60 yd^3/hr)		✓	✓	
Concrete removal (stage 2)	1.06 m^3/hr (1.39 yd^3/hr)		×	✓	
Rebar inspection	18.6 m^2/hr (200 ft^2/hr)		×	✓	
Rebar replacement	0.50 m^2/hr (5.38 ft^2/hr)		×	✓	
Concrete replacement	3.06 m^3/hr (4.00 yd^3/hr)		✓	✓	
Protection board install	24 m^2/hr (200 ft^2/hr)		✓	✓	Area x 2

The repair procedure for protected concrete liner consists of protection board removal, concrete repair, and reinstallation. The installation rate is based on a FireMaster ® installation process of 24 m^2 boards on the curved tunnel wall(Morgan Advanced Material n.d.). To be conservative the removal rate is assumed to be equal to the installation rate. To ensure remediation following a fire event the removal (and installation) area is assumed to be doubled for cases of moderate and heavy damage, as noted in the comments in The post-fire tunnel repair requirements are based on the preceding damage assessment. The concrete tunnel liner can be discretized and the damage level and associated repair requirement for each element can be determined. The overall tunnel closure time can be determined by applying estimated rehabilitation rates as noted in Table 11Error**! Not a valid bookmark self-reference.**. These values are based on authors' engineering judgment as no detailed specifications for tunnel fire repair is available according to a MassDOT (2021) investigation (Gerasimidis and Civjan n.d.).

Table 11. For the concrete liner, no action is needed for the superficial damage as in the definition; concrete-related repair is required for moderate damage, while both the concrete and rebar repair are needed for the heavy damaged class. The rate of each repair step is based on data from an authorized contractor for PennDOT, the shotcrete application rate noted in the Standard Practice for Shotcrete by the US Army Corps of Engineers (1993) (US Army Corps of Engineers 1993)), and the hydro-demolition concrete removal applied in the Channel tunnel repairment after the 2008 fire hazard (Freyssinet Corporation 2021). Figure 25 (c) illustrates the repair time for each discretized tunnel liner segment with the damage state in Figure 25 (b).

For specific tunnel fire hazards, the entire tunnel closure time T_{hr} (hr) for repairment is then calculated by summing the repair time for each discretized tunnel concrete liner element via Eq. (24):

$$T_{hr} = \sum_{1}^{n_2} t(dm_2) + \sum_{1}^{n_3} t(dm_3) \tag{24}$$

where n_1, n_2, and n_3 are the number of panels of superficial, moderate, and heavy damage; $t(dm_j)$, j=1, 2, 3 represents the time to repair the discretized concrete liner of each damage state. The superficial damage does not require post-fire rehabilitation and is therefore omitted from consideration in Eq. (24).

2.2.4.2. Repair cost

The tunnel repair cost following a fire event directly relates to the damage state of the tunnel liner which is estimated via the procedure introduced in section 2.2.4.1. Similar to the tunnel closure time, the repair cost is calculated as the summation of the cost for each discretized tunnel liner segment ($rc(dm_j)$, j=1, 2, 3) and the fixed cost rc_{fix} associated with construction site equipment as expressed in Eq. (25).

$$RC = \sum_{1}^{n_2} rc(dm_2) + \sum_{1}^{n_3} rc(dm_3) + rc_{fix} \tag{25}$$

where n_1, n_2, and n_3 are the number of panels of superficial, moderate, and heavy damage. The value of $rc(dm_j)$ varies with respect to the protection material while rc_{fix} is related to the highest level of concrete liner damage.

The assumption is made that the fire protection board in the region of the fire event is removed for concrete liner inspection and is replaced with new elements. Based on the economic feasibility study of fire protection board in tunnels by Roland L. et al. (Leucker n.d.)., the cost for concrete repair which includes cleaning, high-pressure blasting, chiseling, and shotcrete repair is suitable for the moderate damage defined in this study. The additional cost of reinforcement replacement for heavy damage scenarios can be accounted for. Table 12 lists the detailed area-dependent cost which enables flexible calculation of the repairing cost for various situations. Figure 26 (d) presents the repairing cost of each discretized tunnel liner segment with the damage state in Figure 26 (b).

Table 12: Repairing cost for protected tunnel concrete liner

Fire protection board					
	6mm	9mm	12mm	20mm	Applied to Moderate and Heavy damage region
Protection board material cost	\$41.31/m^2	\$65.80/m^2	\$87.26/m^2	157.02/m^2	
Protection board removal fee	\$81.36/m^2				
Protection board replacement fixed fee	\$5,811.7				
Protection board installation fee	\$81.36/m^2				
Tunnel concrete liner repairment cost					
Superficial damage: None	None				
Moderate damage: Cleaning, high-pressure blasting, chiseling, shotcrete	\$139/m^2+\$29,000 fixed cost				Fixed cost relates to the highest damage level
Heavy damage: Cleaning, high-pressure blasting, chiseling. Reinforcement, shotcrete, repair, joint repair	\$267/m^2+\$81,200 fixed cost				

2.2.4.3. Traffic-related loss

Closing the tunnel for repair after a fire hazard leads to the traffic detour. The corresponding economic loss includes the additional expenditure on time and fuel. Additionally, the unexpected traffic division may cause traffic jams which further increase the time loss. hence, the total tunnel traffic-related economic loss can be calculated via Eq. (26):

$$\begin{aligned} TC_{total} &= TC_{DT} + TC_{DF} + TC_{jam} \\ TC_{DT} &= \left(\sum \frac{DL}{V_i} \times TL_i \times AADT_i\right) \times T_{day} \\ TC_{DF} &= \left(\sum DL \times FL_i \times AADT_i\right) \times T_{day} \\ TC_{jam} &= \left(\sum T_{jam} \times TL_i \times AADT_i\right) \times T_{day} \end{aligned} \tag{26}$$

where TC_{total}, TC_{DT}, TC_{DF}, and TC_{jam} (USD) are the total traffic-related cost, detour time loss cost, detour fuel loss cost, and time loss due to traffic jams. DL (km) represents the detour length; V_i (i=1,2,…) is the traveling speed (km/hr) for different types of vehicles; TL_i (USD) is the hourly rate for each type of vehicle. It is assumed that each car is occupied by one person, and the statutory minimum wage is considered as the hourly rate for this person. FL_i (USD/km) account for the fuel combustion differential for each vehicle type; $AADT_i$ represent the corresponding annual average daily traffic. T_{jam} (hr) is the time of traffic jam due to the unexpected traffic division. T_{day} (days) is the period of tunnel repairment, which depends on the tunnel closure time T_{hr} calculated in section 2.2.4.1. according to the tunnel fire impact and selected protection method. The detailed parameters for traffic-related economic loss are listed in Table 13. To note, the tunnel traffic (including the volume (AADT) and compensation) and the detour length should be implemented here depending on the specific tunnel location and usage.

Table 13: Parameters for traffic-related economic loss assessment

	Small vehicles (≤ 3.5t)	Large vehicles (>3.5t)
Detour time loss (USD/hr)	10.25	23.2
Detour fuel cost (USD /km)	0.35	0.75
Travel speed (km/hr)	80	50
Traffic jam time (hr/day)	0.5	
Tunnel closure days	Determined by tunnel damage	

2.2.4.4. Associated uncertainties

The tunnel damage and corresponding tunnel closure time for a given fire intensity (usually expressed as peak heat release rate) are greatly influenced by the fire-related parameter: total combustion energy and tunnel-related conditions such as the effect of longitudinal ventilation and FFFS if present. As the longitudinal ventilation system is designed to provide critical air velocity, which is consistent with the application scope of the wind-tilt CDSF model, the effect of the ventilation system on the thermal impact is considered to be deterministic. The activation time of the longitudinal ventilation can be assumed to be negligible according to the Burnley tunnel fire event of March 2007 (Beard and Carvel 2005).

The combustion energy, which determines the thermal impact duration, varies according to vehicle type (e.g., car, bus, HGV, and tanker truck) and the combustion material present in each type. For specific fire hazards, the combustion energy is randomly selected between the "lower bound" and "upper bound", which are derived from two sets of data (data by Ingason (Ingason 2009) for the upper bound and by Qi. et al. (Guo et al. 2020b) for lower bound), following a normal distribution. The expressions for "upper bound" E_{tot}^{up} (GJ) and "lower bound" E_{tot}^{low} (GJ) are considered as a function of the peak heat release rate $\dot{Q}_{max}$ (MW) respectively in Eq. (27) and presented in Figure 26 (a).

$$E_{tot}^{up} = 4.9\dot{Q}_{max} - 24.13$$
$$E_{tot}^{low} = 16.47e^{0.01257\dot{Q}_{max}} \quad (27)$$

The FFFS is assumed to suppress the fire intensity while attenuating the radiative and convective heat transfer. According to the latest version of NFPA 502 (version 2020), the HRR reduction factors arise for larger vehicle fires. For each type of vehicle fire (i.e., car, bus, HGV, and tanker truck) with the recommended design fire intensity, an interval that indicates the reduction boundary is provided based on experimental data. Figure 26 (b) shows the lower and upper bound of the reduction factor as a function of the fire heat release rate along with the mean value. The normal distribution was assumed for the reduction factor with standard deviation calculated as one-third of the difference between the upper and lower bounds.

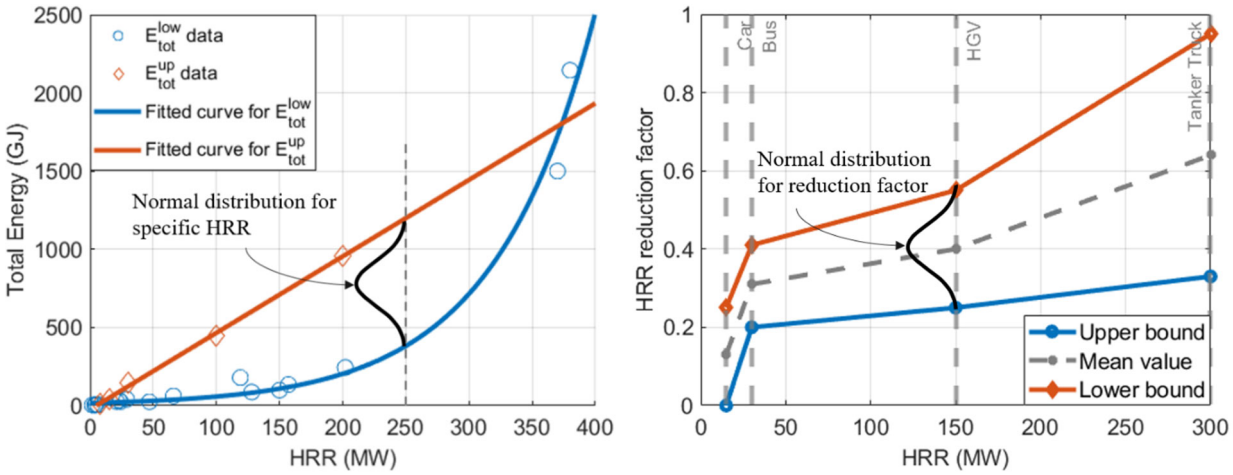

(a) Total combustion energy (b) HRR reduction due to FFFS

Figure 26: Uncertainties associated with tunnel fire impact

The transmission of thermal radiation from the fire to the tunnel surface is reduced by the absorption and scattering of radiation by the droplets in the water spray. Experiments have shown that radiative attenuation ranges from 50% to 83% depending on the type of water spray system, water pressure, and droplet size. To avoid the complexity of accounting for these factors, a conservative value of 40% is applied as the attenuation factor for both radiative and convective thermal impact if the FFFS is installed.

To summarize, the uncertainties in quantifying the tunnel structural damage, closure time, and the corresponding economic loss as subjected to the fire hazard of specific intensity (expressed with HRR) are considered via Monte Carlo Simulation with Latin hypercube sampling, which is highlighted with the greening region in the flowchart in Figure 17. A confidence interval (i.e., 95%) could be selected to provide a reasonably conservative estimation.

2.2.4.5. Life-cycle loss assessment

The expected economic loss due to tunnel vehicle fire hazard is assessed by correlating the loss for specific fire intensity, which is calculated following the steps introduced in section 2.2.4.1 through section 2.2.4.4, with the occurring probability as the expression in Eq. (28).

$$EL = \int \left[TC_{total}(HRR_j) + RC(HRR_j)\right] \cdot p\left(HRR_j\right) \cdot dHRR_j \tag{28}$$

where HRR_i is the heat release rate defining the fire intensity; $TC_{total}(HRR_j)$ and $RC(HRR_j)$ are the traffic-related cost and repairing costs for fire hazards of HRR_i respectively. As introduced in section 2.2.4.4, the conservative values representing a confidence interval could be selected via stochastic analysis.

During the service lifetime of the tunnel, multiple fire hazards may occur, which makes the present value calculation necessary for fire protection method efficiency comparison as well as being consistent with the lifecycle investment calculation. The tunnel fire frequency within a time frame, F_f, can be calculated via

Eq. (29) by considering the fire rate R_f (per million vehicle-km), tunnel traffic volume $AADT$ of all types of vehicles within a given time frame (in billion vehicles), and tunnel length L (in km).

$$F_f = R_f \times AADT \times L \times 365 \tag{29}$$

The return period is then taken as $1/F_f$. It is assumed that the fire hazard occurs in the first year and iteratively happens with the interval of the return period during the tunnel lifetime. Consistent with the present investment, the interest is taken as 1.75% to calculate the total present economic loss in the tunnel lifetime.

2.2.5. Mitigation optimization

The tunnel fire protection method, according to the NFPA 502 should be able to (1) support firefighter accessibility, (2) minimize economic impact, and (3) mitigate structural damage. In practical engineering projects, the investment in fire protection is a concern that should be minimized to increase protection efficiency. Translating to a mathematical problem that can be solved with algorithms, the selection of tunnel fire protection is a multi-objective optimization process.

2.2.5.1. Selected objectives and constraints

The objectives of the tunnel fire protection plan could be flexible according to the necessity of specific projects. In this study, two sets of objectives are applied for comparison. In the first set, minimizing the lifecycle investment calculated according to section 2.2 and minimizing the lifecycle economic loss accessed in section 2.3 are used as objectives. In the second set, the first objective is the overall financial flow, including both investment and loss, which is used in the economic feasibility study by Roland L. et al.(Leucker n.d.), and the second is the protection efficiency in reducing the economic loss compared to the non-protection case. The objective of mitigating the structural damage by NFPA 502 is omitted because the structural damage is largely represented by economic loss according to the procedure introduced in section 2.3.

The most straightforward constraint for the optimization is setting the budget for the fire protection plan, which is often a constraint of practical engineering projects. Moreover, to realize the firefighter accessibility goal, the installation of tunnel longitudinal ventilation could be used as a constraint.

2.2.5.2. Pareto front development with genetic algorithm

The genetic algorithms (GAs) have become the most popular choice in optimization with conflicting objectives (i.e., minimize the investment and minimize the economic loss in this study). It has been used in many fields of science, including engineering, economics, and logistics where optimal decisions need to be taken in the presence of trade-offs between objectives. Generally, this algorithm repeatedly evaluates the objectives at several trial points of the admission domain with several iterations (called “generations”) and

provides the Pareto front that contains the optimal solutions. These solutions can be used as the reference for the final decision-making process.

2.3. Case study

The performance-based tunnel fire mitigation optimization method introduced in section 2.2 is applied to the Lehigh Tunnel southbound for illustration purposes. The factors influencing the optimal solutions such as tunnel dimension, traffic volume and composition, and detour length are studied in the sensitivity analysis in the following section.

2.3.1. Prototype tunnel

A previous investigation of the shape and dimension of tunnels in the United States (Guo et al. 2019) showed that a typical roadway tunnel has a road width ranging from 8 to 13 m (26.2-42.7 ft), accommodates 2 to 3 travel lanes, and has a curved ceiling. The recent development and deployment of tunnel boring machines have made circular tunnel cross-section more common and likely will become the dominant tunnel cross-section in the future. Consequently, this section focuses on Lehigh Tunnel (southbound), which is a typical two-lane circular tunnel, as shown in Figure 27. The height of the tunnel is H_T=7.78 m while the corresponding tunnel radius is R_T=5.28 m. The tunnel length is 1335.6m (4382ft). According to the National Tunnel Inventory database, the AADT of the south Lehigh Tunnel is 13099 vehicles/day, while the detour length is merely 1 mile. The fire rate (R_f) is accessed according to data from a study published in 2016 by PIARC (PIARC Technical Committee 3.3 2016). The composition of the tunnel traffic is based on the information provided by PennDOT in 2019 for a two-lane urban tunnel in Pennsylvania (Guo et al. 2020b) and labeled as Traffic 2 in Table 14. The corresponding continuous tunnel fire HRR probability density distribution and cumulative density distribution are derived via Monte Carlo Simulation with the equation correlating the combustion weight with HRR value (Guo et al. 2021a) and presented with solid lines (black and gray, respectively) in Figure 28. Traffic 1 Traffic 3, and Traffic 4 listed in Table 14 and presented in Figure 28 with dash lines are developed by varying the percentage of the truck (i.e., decrease to 0.00% or increase to 20% and 50%) for sensitivity analysis in the following sections.

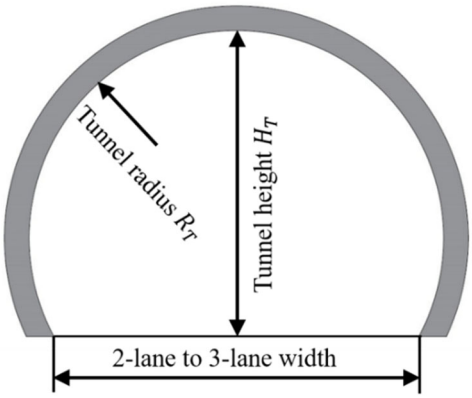

Figure 27: Circular tunnel cross-section

Table 14: Typical 2-lane traffic composition and fire rate

Vehicle type	Traffic composition				Fire rate
	Traffic 1	Traffic 2	Traffic 3	Traffic 4	
Motorcycle:	1.80%	0.35%	0.00%	0.00%	9.56
Car:	80.50%	79.05%	68.00%	42.5%	
Pick-up Truck:	15.40%	13.99%	12.00%	7.5%	
Bus:	2.40%	0.99%	0.00%	0.00%	
HGV:	0.00%	5.60%	20.00%	50.00%	

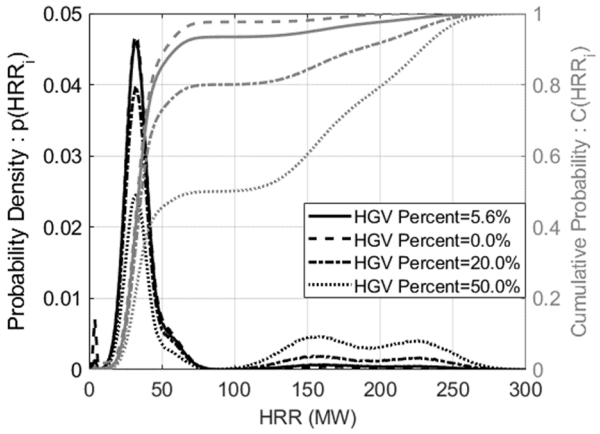

Figure 28: HRR probability distribution based on tunnel traffic

2.3.2. Optimization problem set up

The tunnel fire protection may consist of both active and passive approaches. For active protection, two design variables α_{LV} and α_{FFFS} are assigned to represent the existence of longitudinal ventilation and FFFS, respectively. These two parameters are binary chosen from either 1 or 0, representing installation or not, respectively. For passive fire protection, only the protection board is considered in this case study. The variable α_{PB} is an integer selected from 0, 1, 2, 3, 4, 5 representing no protection, 8mm, 12mm, 15mm, 18mm, and 20mm board. The associated damage assessment map for each thickness is developed in section 2. The lifecycle Cost and Loss due to tunnel fire hazards for a specific protection plan are represented as *C*

and L, while the L_0 is the loss for the case of no protection. Therefore, the formulation of the optimization problem is:

Find

$$\alpha_{LV}, \alpha_{FFFS}, \text{and } \alpha_{PB}$$

So that

Objective sets 1		Objective sets 2
C=minimize	Or	$C+L$=minimize
L=minimize		$\frac{L_0-L}{C}$=maximize

Subjected to the constraining

$$\alpha_{LV} = 0 \text{ or } 1$$

$$\alpha_{FFFS} = 0 \; or \; 1$$

$$\alpha_{PB} = 0,1,2,\dots,5$$

$$\frac{L_0-L}{C} \geq 0 \text{ for objective set 2}$$

The constrain can be modified according to the tunnel conditions or specifications. For example, $\alpha_{LV} = 1$ if the longitudinal ventilation system is required to control the smoke and ensure life safety. This is illustrated in the results for comparison.

2.3.3. Results and discussion

As presented in Figure 29a, the Pareto fronts containing the optimal solutions are provided via GAs for objective set 1. The gray circles represent every individual protection solution, while the red triangular and blue squares indicate the non-constrain case (the longitudinal ventilation is not strictly required) and the longitudinal ventilation installed case for smoke control according to the NFPA 502, respectively. For the non-constrain case, 12 optimal solutions are identified. The leftmost solution (marked as S1) in Figure 29a represents the case of no protection; as a result, the economic loss is the highest. Gradually installing the protections, the economic loss drops, as illustrated in the solution marked as S2 (no ventilation system and FFFS installed; 15mm thick protection board) and S3 (no ventilation; FFFS installed; 20 mm thick protection board). Constrained with the requirement of longitudinal ventilation installation, the optimal solutions are reduced to 8 cases. Generally, most of the longitudinal ventilation included solutions are not optimal for the non-constrain case for its significant investment. For the solution marked as S4, no FFFS or fire protection board is implemented; and for S5, a 12 mm thick fire protection board is installed while the FFFS is not. For the solution of S6, which is on the Pareto front of both non-constrain and constrained cases, both the longitudinal ventilation and FFFS are installed, while the protection board is as thick as 20mm. This mitigation plan ensures the structural safety of the southbound Lehigh Tunnel and requires no post-fire structure repair. The optimal solutions are listed in Table 15. To conclude, the longitudinal

ventilation, which is required for the sake of life safety, is not as efficient as the FFFS and protection board to mitigate the tunnel fire damage and associated economic loss.

Figure 29b presents the Pareto front using objective set 2 with the optimal solutions listed in Table 15. Compared to objective 1, the optimal solutions are fewer for non-constrain, and longitudinal ventilation installed cases. The solution marked as S1 represents the FFFS installations, while S2 contains no protection. For the longitudinal ventilated installed case, S3 represents the FFFS installation. Overall, objective set 2 is more efficient in narrowing down the number of choices, which provides convenience for decision-making.

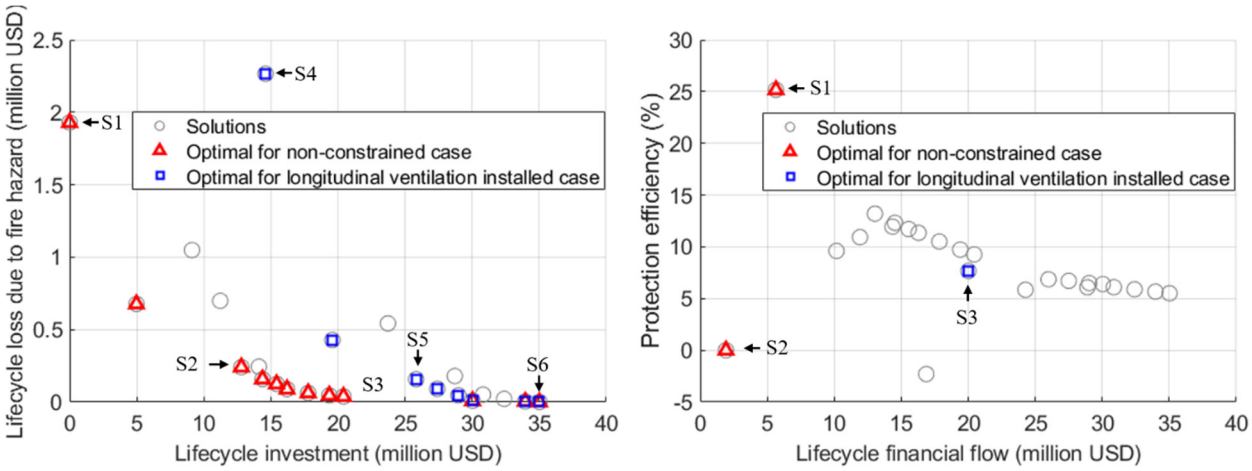

(a) Objective set 1 (b) Objective set 2

Figure 29: Pareto front generated via genetic algorithm for southbound Lehigh Tunnel

Table 15: Optimal fire protection for southbound Lehigh Tunnel

Protection Options		Objective set 1																			Objective 2		
		Non-constrain												Ventilation Installed								Non-constrain		Ventilation Installed
		1 (S1)	2 (S2)	3	4	5	6	7	8	9 (S3)	10	11	12	1 (S4)	2 (S5)	3	4	5	6	7	8 (S6)	1 (S2)	2 (S1)	1 (S3)
Longitudinal ventilation											✓	✓	✓				✓							✓
FFFS installation						✓	✓	✓	✓	✓		✓	✓						✓	✓	✓		✓	✓
PB thickness (mm)	8																							
	12						✓								✓									
	15		✓					✓								✓								
	18			✓					✓			✓					✓			✓				
	20				✓					✓	✓		✓					✓				✓		

2.4. Sensitivity analysis

As aforementioned, the factors influencing the decision of the tunnel fire protection plan include the tunnel dimension (i.e., cross-section and tunnel length), traffic (i.e., volume and composition), and the importance of the traffic network (i.e., detour length). The sensitivity analysis in this section uses the southbound Lehigh Tunnel with no constrain in the longitudinal ventilation as the base to study the impact of these parameters. Objective set 2 is applied.

2.4.1. Influence of tunnel dimension

The size of the tunnel generally influences the fire impact magnitude and the investment in fire protection. According to the NTI database, most US circular tunnels are two-lane tunnels, whose dimensions vary slightly based on the shoulder and width of the lanes. However, the three-lane tunnel driven by the tunnel boring machine is becoming more common, for example, the Xiamen Xiang'an Tunnel in China. The length of the tunnel varies from 3.35m (11ft of Apishapa Arch) to 4053m (13300ft of Anton Anderson Tunnel). Hence, a typical three-lane (H_T=9.93 m R_T=6.98 m) circular cross-section and tunnel length of 100m, 200m, 800m, 1600m, and 3200m are selected for sensitivity analysis.

The optimal solutions for the 3-lane circular tunnel are almost consistent with that for the 2-lane tunnel as presented in Figure 30a. For the longitudinal ventilation installed case, the solution of only longitudinal ventilation installation is added. This solution is not optimal for the 2-lane tunnel for its larger confinement effect on the fire hazard, which leads to negative protection efficiency.

As presented in Figure 30b, the length of the tunnel does not strongly influence the optimal solutions mainly because the investment in fire protection is almost proportional to the tunnel length (i.e., the number of jet fans, the area of fire protection board, and the installation of FFFS). Meanwhile, the protection efficiency decreases for a higher chance of fire hazards via Eq. (29).

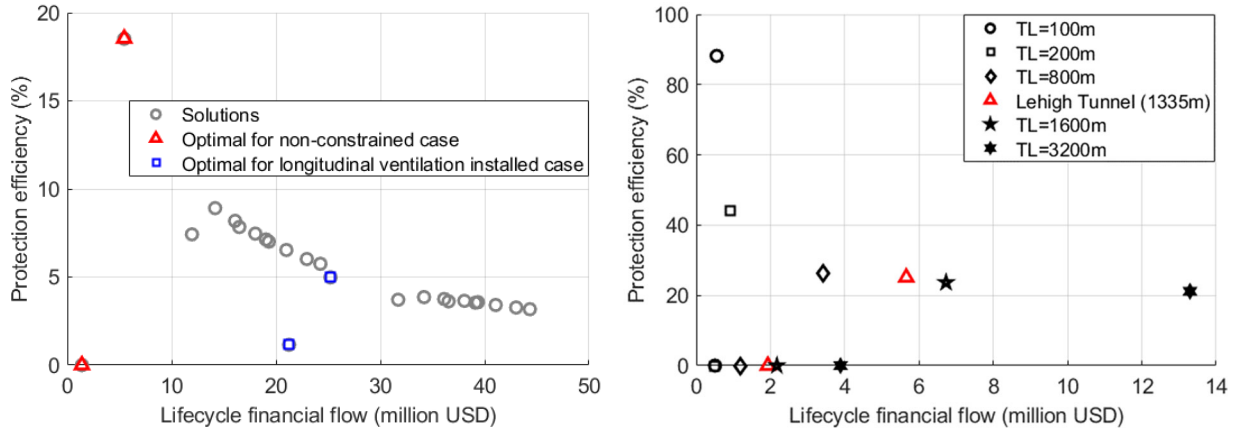

(a) Tunnel cross-section (b) Tunnel length

Figure 30: Influence of tunnel dimension on optimal fire mitigation

2.4.2. Influence of traffic

In the procedure of determining the tunnel fire loss, the tunnel traffic influence the fire frequency, the overall expected tunnel fire impact intensity, and economic loss due to the tunnel closure. The traffic volume of tunnels in the US varies widely from below 100 (i.e., McCoy's Ferry tunnel) to over 250,000 vehicles/per day (i.e., Yerba Buena Crossing Tunnel) according to the NTI database for 2022. The percentage of the truck fluctuates from 0% (NJ 29 tunnel) to 50% (i.e., Green River Tunnel) for tunnel used for mixed traffic types and increases to over 90% for tunnel constructed for buses and trucks' transportation (i.e., COLLEGE HILL BUS TUNNEL). Accordingly, the AADT of the prototype two-lane circular Lehigh Tunnel is amplified and scaled down by 5 and 20 times; the percentage of the HGV in the traffic composition is reduced to 0% and increased to 20% and 50% with the HRR probability density curves displayed in Figure 28.

Presented in Figure 31 (a) and listed in Table 16, amplifying the AADT by five times, the none-protection solution is not optimal as the fire frequency increases. For the case of increasing the AADT by 10 and 20 times, the fire protection board is included in the mitigation plan. As a trend, the heavier the traffic is, the thicker the protection board is preferred. The benefit (indicated by protection efficiency) of introducing fire protection dramatically increases for tunnels with heavy traffic.

The percentage of the HGVs generally influences the expected consequences (i.e., damage and corresponding repairing cost and time). The optimal solutions remain unchanged for the HGV percentage from 0.0% to 20%, while the protection efficiency increases. In the case that the HGV percentage increases to 50%, the none-protection solution is not optimal.

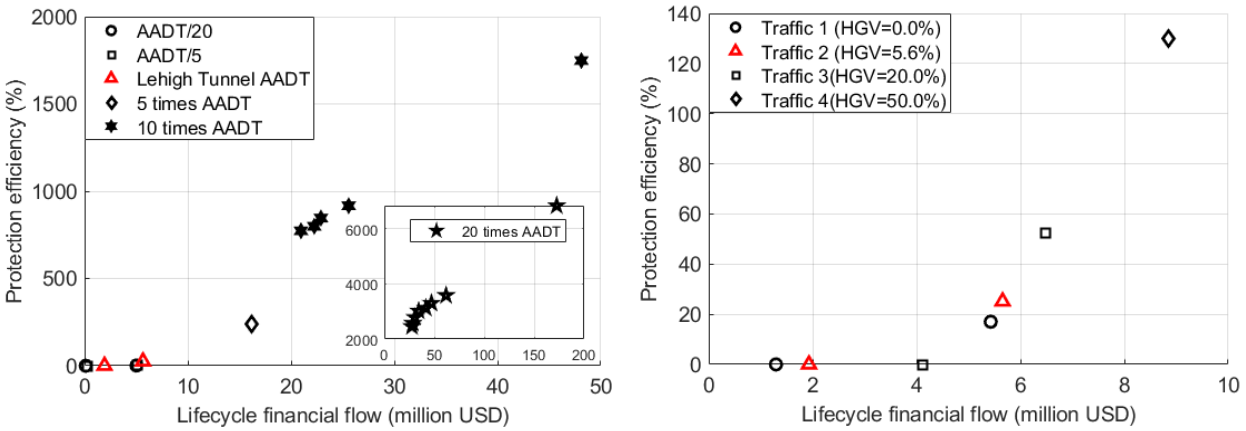

(a) Vary AADT (b) Vary traffic composition

Figure 31: Influence of tunnel traffic on optimal fire mitigation

Table 16: Optimal solutions influenced by traffic volume

AADT	Optimal solution number	Protection Plans			Lifecycle flow (million USD)	Protection efficiency (%)
		Ventilation	FFFS	Protection Board thickness (mm)		
655	1	Natural	No	None	0.11	0.00
	2	Natural	Yes	None	5.03	1.23
2620	1	Natural	No	None	0.24	0.00
	2	Natural	Yes	None	5.08	2.98
13099	1	Natural	No	None	1.93	0.00
	2	Natural	Yes	None	5.66	25.15
65495	1	Natural	No	15	16.22	236.26
130990	1	Natural	No	15	25.58	916.70
	2	Natural	No	18	22.90	846.04
	3	Natural	No	20	22.25	798.94
	4	Natural	Yes	None	48.12	1748.53
	5	Natural	Yes	12	20.96	773.13
261980	1	Natural	No	15	61.85	3584.57
	2	Natural	No	18	47.19	3299.77
	3	Natural	No	20	41.57	3123.46
	4	Natural	Yes	None	172.55	6840.29
	5	Natural	Yes	12	34.45	3017.68
	6	Natural	Yes	15	30.65	2786.19
	7	Natural	Yes	18	28.58	2577.32
	8	Natural	Yes	20	27.67	2456.04

2.4.3. Influence of tunnel detour length

The detour length directly affects the traffic-related loss calculated via Eq. (28). It should be decided according to the possible alternative route if the tunnel is closed. For the Lehigh Tunnel, the 1.6 km (1 mile)

detour length is small, but it could increase to 320 km (199 miles) for Zion-Mount Carmel Tunnel) and 684 km (425 miles) as for Thimble Shoal Tunnel. For some tunnels (i.e., Portage Creek Tunnel) there is even no alternative pass. Figure 32 shows the Pareto fronts for the cases where the detour length increases from 1.6 km for the Lehigh tunnel to 50 km, 320 km, 700 km, and 1000 km, which represent the case that detour does not exist, with all the optimal solutions listed in Table 17. As a trend, more fire protection is needed as the detour length increase. For example, the none-protection solution is eliminated as the detour length increases to 50 km; the fire protection board starts to reveal its efficiency for the detour lengths of 320km or 700km; the longitudinal ventilation, though, is not economically efficient enough to mitigate tunnel structural damage, is included in the optimal solutions for the none-detour case.

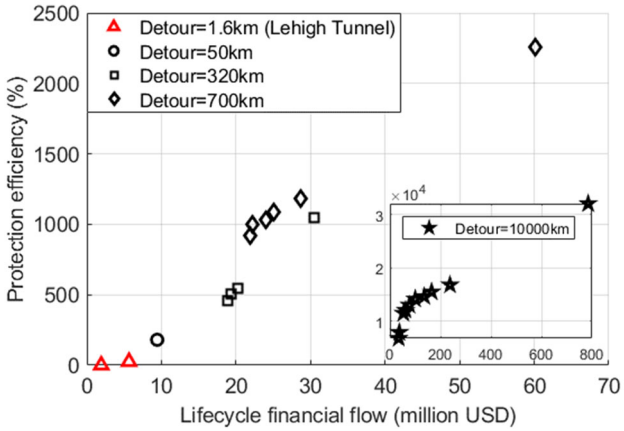

Figure 32: Influence of tunnel importance on optimal fire mitigation

Table 17: Optimal solutions for tunnel with various detour lengths

Detour Length (km)	Optimal solution number	Protection Plans			Lifecycle flow (million USD)	Protection efficiency (%)
		Ventilation	FFFS	Protection Board thickness (mm)		
1.6 (Lehigh)	1	Natural	No	None	1.93	0.00
	2	Natural	Yes	None	5.66	25.16
50	1	Natural	Yes	None	9.43	180.36
320	1	Natural	No	15	20.19	547.15
	3	Natural	No	18	19.32	505.34
	4	Natural	Yes	None	30.47	1043.02
	5	Natural	Yes	12	18.96	460.99
700	1	Natural	No	15	28.74	1184.61
	2	Natural	No	18	25.07	1089.62
	3	Natural	No	20	23.95	1030.88
	4	Natural	Yes	None	60.07	2259.90
	5	Natural	Yes	12	22.13	996.42
	6	Natural	Yes	15	21.96	919.91
10000	1	Natural	No	15	238.04	16781.18

2	Natural	No	18	165.17	15483.22
3	Natural	No	20	135.88	14617.89
4	Natural	Yes	None	785.04	32027.33
5	Natural	Yes	12	100.06	14135.92
6	Natural	Yes	15	76.92	13006.13
7	Natural	Yes	18	61.73	12035.95
8	Natural	Yes	20	53.58	11471.75
9	Longitudinal	No	20	37.19	7891.95
10	Longitudinal	Yes	20	35.02	6783.40

2.5. Conclusion

This study presents a decision-making methodology to optimize the fire mitigation method for roadway tunnels by both minimizing the lifecycle financial cost including the investment and economic loss while maximizing the protection efficiency. The optimization accounts for the performance of the tunnel structure subjected to fire hazard, the post-fire repair procedure, the tunnel traffic, and its importance. These variables are used to develop optimal active and passive fire protection method for the structure studied. The conclusion of this study are as follows:

- The MATLAB-SAFIR method is efficient to model the behavior of the concrete liner protected with passive fire protection subjected to fire hazards. Considering the uncertainties associated with the thermal parameters of both concrete liner and protection materials with MCS, the damage maps are developed to help efficiently characterize the damage state of the protected concrete liner.
- With the computational efficiency of the confined discretized solid flame (CDSF) model and damage maps developed in this study, the entire tunnel damage along with the repairing time and cost afterward, can be assessed as subjected to specific tunnel fire hazard.
- The lifecycle investment for a specific fire protection plan is calculated, containing the installation and maintenance fee, while the lifecycle loss due to the tunnel fire hazard is assessed based on the tunnel traffic and its importance. The uncertainties associated are considered via MCS taking the 95% confidence interval.
- The multi-objective optimization via GAs provides optimal solutions while contradictory objectives are applied. This optimization method is flexible in choosing the objectives and constraints as needed according to specific engineering requirements. Carefully choosing the appropriate objective sets can help narrow down decision-making choices.

The factors influencing the optimal solutions include the tunnel traffic and the detour length. Generally, tunnel of smaller size, higher traffic volume, higher HGV percentage, longer detour length requires more

protection. The longitudinal ventilation, though required for life safety concerns, is not efficient for mitigating the tunnel structural damage compared to the FFFS and protection boards.

REFERENCE

AESTUVER. n.d. “SDB_ AESTUVER Tx fire-protection board for tunnels.”

ANSI C80.1. 2005. *American National Standard for Electrical Rigid Steel Conduit (ERSC)*. NEMA Standards Publication.

Anurag, J. 2017. “IMPACT OF FIXED FIREFIGHTING SYSTEMS ON ROAD TUNNEL RESILIENCE.” The University of North Carolina at Charlotte.

ASTM International. 2016. “ASTM E1529 Standard Test Methods for Determining Effects of Large Hydrocarbon Pool Fires on Structural Members and Assemblies.” https://doi.org/10.1520/E1529-16.

ASTM International. 2019. *E136-19a Test Method for Assessing Combustibility of Materials Using a Vertical Tube Furnace at 750C*. West Conshohocken, PA: ASTM International.

Beard, A., and R. Carvel (Eds.). 2005. *The handbook of tunnel fire safety*. London, UK: Thomas Telford.

Bechtel/Parsons Brinckerhoff., and Bechtel/Parsons Brinckerhoff. 1995. *Memorial Tunnel Fire Ventilation Test Program: Test Report*. Boston, MA: Massachusetts Highway Department, FHWA.

Bergeson, W., and S. Ernst. 2015. *Tunnel Operations, Maintenance, Inspection, and Evaluation (TOMIE) Manual*. 263. Washington DC 20590.

Bergmeister, K., P. Brunello, M. Pachera, F. Pesavento, and B. A. Schrefler. 2020. “Simulation of fire and structural response in the Brenner Base Tunnel by means of a combined approach: A case study.” *Engineering Structures*, 211: 110319. https://doi.org/10.1016/j.engstruct.2020.110319.

CEN. 2002. *Eurocode 1: Actions on structures -Part 1-5: General actions - Actions on structures exposed to fire*. Brussels, Belgium: European Committee for Standardization.

CEN. 2005. *EN 1993-1-2:2005 Eurocode 3: Design of steel structures - Part 1-2: General rules - Structural fire design*. Brussels, Belgium: European Committee for Standardization.

CEN. 2008. *EN 1992-1-2: Eurocode 2: Design of concrete structures - Part 1-2: General rules - Structural fire design*. Brussels, Belgium: European Commission for Standardization.

CEN. 2009. *Eurocode 1: Actions on structures - Part 1-2: General actions - Actions on structures exposed to fire*. Brussels, Belgium: European Committee for Standardization.

CoDOT. n.d. “Tunnel Systems Estimates.”

Commonwealth of Pennsylvania. 2016. *PennDOT Specifications*. Publication 408.

Cortes, C., and V. Vapnik. 1995. “Support-Vector Networks.” *Machine Learning*, 20 (3): 273–297. https://doi.org/10.1007/BF00994018.

Dipl.-Ing, M. L., and T. B. Dipl.-Ing. n.d. *Fixed Fire Fighting Systems for Road and Rail Tunnels*. Cologne/D: Fogtec Fire Protection.

European Committee for Standardization. 2004. *Eurocode 2: Design of Concrete Structures - Part 1-2: General Rules - Structural Fire Design*.

fermacell AESTUVER Fire safety concepts for underground transport systems. n.d. Aestuver.

Franssen, J. M., and T. Gernay. 2016. “USER’S MANUAL FOR SAFIR 2016c A COMPUTER PROGRAM FOR ANALYSIS OF STRUCTURES SUBJECTED TO FIRE.” UNIVERSITY OF LIEGE Department ArGEnCO Service Structural Engineering.

Franssen, J.-M., and T. Gernay. 2017. “Modeling structures in fire with SAFIR®: theoretical background and capabilities.” *Journal of Structural Fire Engineering*, 8 (3): 300–323. https://doi.org/10.1108/JSFE-07-2016-0010.

Freyssinet Corporation. 2021. *Concrete Repair & Tunnel Strengthening: Channel Tunnel Fire Damage Repair*. United Kingdom.

Gehandler, J. 2015. "Road tunnel fire safety and risk: a review." *Fire Science Reviews*, 4 (1): 2. https://doi.org/10.1186/s40038-015-0006-6.

Gerasimidis, S., and S. Civjan. n.d. *Post-Fire Damage Inspection of Concrete Structures*. University of Massachusetts Amherst;UMass Transportation Center.

Guo, Q., A. Carlton, S. E. Quiel, and C. J. Naito. 2020a. "Stochastic Thermal Demand and Resulting Capacity Loss of Concrete Tunnel Liners Subjected to Vehicle Fires." *Transportation Research Record*, 2674 (5): 293–304. https://doi.org/10.1177/0361198120914612.

Guo, Q., A. Carlton, S. E. Quiel, and C. J. Naito. 2020b. "Stochastic Thermal Demand and Resulting Capacity Loss of Concrete Tunnel Liners Subjected to Vehicle Fires." *Transportation Research Record*, 2674 (5): 293–304. SAGE Publications Inc.

Guo, Q., S. E. Quiel, and C. J. Naito. 2021a. "Traffic-Based Quantitative Risk Analysis of Structural Fire Damage to 2 Roadway Tunnel Linings." *Structure and Infrastructure Engineering*, Manuscript NSIE-2021-0109: 59.

Guo, Q., S. E. Quiel, and C. J. Naito. 2021b. "Traffic-based quantitative risk analysis of structural fire damage to roadway tunnel linings." *Structure and Infrastructure Engineering*, 1–17. https://doi.org/10.1080/15732479.2021.1993936.

Guo, Q., K. J. Root, A. Carlton, S. E. Quiel, and C. J. Naito. 2019. "Framework for rapid prediction of fire-induced heat flux on concrete tunnel liners with curved ceilings." *Fire Safety Journal*, 109: 102866.

Heskestad, G. 1983. "Luminous heights of turbulent diffusion flames." *Fire Safety Journal*, 5 (2): 103–108.

Holland, C., M. Shipp, and D. Crowder. 2015. *A series of experiments to assess the effect of fire on a selection of electrical cable supports and fixings*. Building Research Establishment, Ltd.

Hua, N., A. Tessari, and N. Elhami Khorasani. 2021. "Characterizing damage to a concrete liner during a tunnel fire." *Tunnelling and Underground Space Technology*, 109: 103761. https://doi.org/10.1016/j.tust.2020.103761.

Ingason, H. 2009. "Design fire curves for tunnels." *Fire Safety Journal*, 44 (2): 259–265.

Ingason, H., Y. Z. Li, and A. Lönnermark. 2011. *Runehamar tunnel fire tests (SP Report 2011:55)*. Boras, Sweden: SP Technical Research Institute of Sweden.

Ingason, H., Y. Z. Li, and A. Lönnermark. 2015a. *Tunnel Fire Dynamics*. New York, NY: Springer New York.

Ingason, H., Y. Z. Li, and A. Lönnermark. 2015b. "Runehamar tunnel fire tests." *Fire Safety Journal*, 71: 134–149.

Ingham, J. 2009. "Forensic engineering of fire-damaged structures." *Proceedings of the Institution of Civil Engineers - Civil Engineering*, 162 (5): 12–17. https://doi.org/10.1680/cien.2009.162.5.12.

Insulationshop.co. n.d. "Masterboard Promat." Accessed July 1, 2022. https://www.insulationshop.co/6mm_masterboard_promat_fire_insulation.html.

Isolatek International. n.d. "ISOLATEK Tunnel Application." Accessed July 1, 2022. https://www.isolatek.com/tunnel/tunnel-application/.

Joint ACI/TMS Committee 216, and Masonry Society (U.S.) (Eds.). 2007. *Code requirements for determining fire resistance of concrete and masonry construction assemblies (ACI 216.1-*

07, TMS-216-07): an ACI/TMS Standard. Farmington Hills, MI: American Concrete Institute.

Jovanović, B., N. E. Khorasani, T. Thienpont, R. K. Chaudhary, and R. Van Coile. 2020. "Probabilistic models for thermal properties of concrete." *Proceedings of the 11th International Conference on Structures in Fire (SiF2020)*. Online: The University of Queensland.

Kennedy, W. D., and J. F. L. Lowndes. 1996. "Critical velocity: Past, present and future." *Smoke and critical velocity in tunnels, Seminar, Smoke and critical velocity in tunnels*. ITC.

Khorasani, N. E., P. Gardoni, and M. Garlock. 2015. "Probabilistic Fire Analysis: Material Models and Evaluation of Steel Structural Members." *J. Struct. Eng.*, 141 (12): 04015050. https://doi.org/10.1061/(ASCE)ST.1943-541X.0001285.

Kodur, V. K. R., and A. M. Shakya. 2013. "Effect of temperature on thermal properties of spray applied fire resistive materials." *Fire Safety Journal*, 61: 314–323. https://doi.org/10.1016/j.firesaf.2013.09.011.

LEE, C. K., R. F. CHAIKEN, and J. M. SINGER. 1979. "Interaction Between Duct Fires and Ventilation Flow: An Experimental Study." *Combustion Science and Technology*, 20 (1–2): 59–72. Taylor & Francis. https://doi.org/10.1080/00102207908946897.

Leucker, R. n.d. "Economic feasibility study for the use of fire protection boards in road tunnels." 9.

Li, Y. Z., C. Huang, J. Anderson, R. Svensson, H. Ingason, B. Husted, M. Runefors, and J. Wahlqvist. 2017. *Verification, validation and evaluation of FireFOAM as a tool for performance design*.

Lönnermark, A. 2005. "On the Characteristics of Fires in Tunnels." Doctoral Dissertation. Lund, Sweden: Lund University.

Lu, F. 2015. "On the prediction of concrete spalling under fire." Switzerland: ETH Zurich.

McGrattan, K. B., H. R. Baum, and A. Hamins. 2000. *Thermal radiation from large pool fires*. Gaithersburg, MD: National Institute of Standards and Technology.

McGrattan, K., R. McDermott, S. Hostikka, and J. Floyd. 2013. *Fire Dynamics Simulator Users Guide, Sixth Edition*. Gaithersburg, MD: National Institute of Standards and Technology.

Morgan Advanced Material. n.d. "FireMaster T-board system curved wall installation." Accessed January 15, 2022. https://www.morganthermalceramics.com/en-gb/resources/videos-and-animations/.

Mosen Ltd. 2022. "Tunnel fire suppression." https://mosen.global/services/tunnel-safety/tunnel-fire-suppression/.

National Fire Protection Association. 2007. *NFPA 130: Standard for Fixed Guideway Transit and Passenger Rail Systems.* Quincy, MA: National Fire Protection Association.

National Fire Protection Association. 2010. *NFPA 130: Standard for Fixed Guideway Transit and Passenger Rail Systems.* Quincy, MA: National Fire Protection Association.

National Fire Protection Association. 2020. *NFPA 130: Standard for Fixed Guideway Transit and Passenger Rail Systems.* Quincy, MA: National Fire Protection Association.

NFPA. 2017. *NFPA 502: Standard for road tunnels, bridges, and other limited access highways*. Quincy, MA: National Fire Protection Association.

Nicholas Carino, M Starnes, John Gross, Jiann Yang, S Kukuck, Kuldeep Prasad, and Richard Bukowski. 2005. "Passive Fire Protection. Federal Building and Fire Safety Investigation of the World Trade Center Disaster (NIST NCSTAR 1-6A)." National Construction Safety

Team Act Reports (NIST NCSTAR), National Institute of Standards and Technology, Gaithersburg, MD.
OBO Betterman. 2019. *Fire protection guide for electrical installations*. Menden, Germany: OBO Bettermann Holding GmbH & Co. KG.
Ohmura, T., M. Tsuboi, M. Onodera, and T. Tomimura. n.d. "Specific Heat Measurement of High Temperature Thermal Insulations by Drop Calorimeter Method." 17.
Ouyang, Z., Q. Guo, S. E. Quiel, and C. J. Naito. 2021. "Vulnerability of Drop Ceilings in Roadway Tunnels to Fire-Induced Damage." *Transportation Research Record*, 03611981211026659. SAGE Publications Inc. https://doi.org/10.1177/03611981211026659.
PIARC. 2007. *Chapter 7: Design Criteria for Structure Resistance to Fire*. PIARC Technical Committee on Road Tunnel Operation.
PIARC. 2022. "Fire Resistance of Equipment." Accessed July 7, 2022. https://tunnelsmanual.piarc.org/en/equipment-systems-mitigation-fire-hazards/fire-resistance-equipment.
PIARC Technical Committee 3.3. 2016. *Experience with Significant Incidents in Road Tunnels*. Paris, France: World Road Association (PIARC).
Pichler, C., R. Lackner, and H. A. Mang. 2006. "Safety Assessment of Concrete Tunnel Linings under Fire Load." *J. Struct. Eng.*, 132 (6): 961–969. https://doi.org/10.1061/(ASCE)0733-9445(2006)132:6(961).
Promat. 2014. "Calcium Silicate Insulation."
Promat. n.d. *Promatect ® Tunnel project references overview*. Promat.
Promat International. n.d. "PROMATECT®-T."
Promat International. n.d. "PROMATECT®-H."
Promat International. n.d. "Promatect-tf-x.pdf."
Schrefler, B. A., P. Brunello, D. Gawin, C. E. Majorana, and F. Pesavento. 2002. "Concrete at high temperature with application to tunnel fire." *Computational Mechanics*, 29 (1): 43–51.
Sýkora, J., D. Jarušková, M. Šejnoha, and J. Šejnoha. 2018. "Fire risk analysis focused on damage of the tunnel lining." *Fire Safety Journal*, 95: 51–65.
Thomas, P. H. 1958. *THE MOVEMENT OF BUOYANT FLUID AGAINST A STREAM AND THE VENTING OF UNDERGROUND FIRES*. Fire Research Note. Fire Research Note 351.
Thomas, P. H. 1968. *THE MOVEMENT OF SMOKE IN HORIZONTAL PASSAGES AGAINST AN AIR FLOW*. Fire Research Note. Fire Research Note 723.
UL Standard. 2017. *UL 2196-Fire Test for Circuit Integrity of Fire-Resistive Power, Instrumentation, Control and Data Cables*.
US Army Corps of Engineers. 1993. *Standard Practice for Shotcrete*. DEPARTMENT OF THE ARMY.
U.S. Army Corps of Engineers. 2008. *User's Guide for the Single-Degree-of-Freedom Blast Effects Design Spreadsheets (SBEDS): PDC TR-06-02 Rev 1*. Washington, D.C.
USDOT. 2015. *Specifications for the National Tunnel Inventory*. Washington, DC: U.S. Department of Transportation; Federal Highway Administration.
Wikipedia. 2021. "2008 Channel Tunnel fire." Accessed August 12, 2021. https://en.wikipedia.org/wiki/2008_Channel_Tunnel_fire.
Wikipedia contributors. n.d. "Pareto front." Accessed July 1, 2022. https://en.wikipedia.org/w/index.php?title=Pareto_front&oldid=1057242200.

Zhu, Z., Q. Guo, S. E. Quiel, and C. J. Naito. 2022. “Rapid prediction of fire-induced heat flux on the liners of horseshoe and circular tunnels with longitudinal ventilation at critical velocity.” *Fire Safety Journal*, 130: 103590. https://doi.org/10.1016/j.firesaf.2022.103590.

Zhu, Z., Q. Guo, S. Quiel, and C. Naito. n.d. “Rapid Prediction of Fire-Induced Heat Flux on the Liners of Horseshoe and Circular Tunnels with Longitudinal Ventilation at Critical Velocity.” *Fire Safety Journal*, under review.

Zhu, Z., S. E. Quiel, A. Carlton, K. A. Mueller, and S. M. Marjanishvili. 2020. “Performance-based prioritisation of fire protection for steel girder overpasses in a complex highway interchange.” *Structure and Infrastructure Engineering*, 16 (3): 394–411. Taylor & Francis. https://doi.org/10.1080/15732479.2019.1666884.

APPENDIX A – TECHNOLOGY TRANSFER ACTIVITIES

1. Accomplishments

1.1 What was done? What was learned?

(1) The confined discretized solid flame (CDSF) model previously developed by the authors can efficiently calculate the incident heat flux on the conduit due to vehicle fires with varying intensities, the range for which is obtained from NFPA 502. Both naturally ventilated and longitudinally ventilated (with airflow at critical velocity) conditions can be considered.

(2) Due to their small thermal mass, the temperature increases in the conduit pipe when subjected to fire is not sensitive to its steel material type or sizing. However, the conduit temperature is significantly affected by the percentage of surface area that is exposed to heating. A conservative correlation is developed to calculate the internal conduit temperature as a function of the incident heat flux and surface area exposure percentage.

(3) The peak total heat flux imparted by the fully developed fire at every tunnel location is associated with a time history per Ingason's quadratic design curve for tunnel fires [33]. The sensitivity of the curve parameters to total fuel load, growth rate, and decay rate were examined. For all vehicle fire scenarios considered in this study, the total duration of thermal exposure does not exceed 2.5 hours. Based on the results, the peak thermal exposure duration for a standard test to determine conduit fire resistance could range from 30 minutes to 2 hours, depending on a user-defined threshold of fire hazard severity.

(4) Based on the results of parametric analyses, the thermal impact on exposed electrical conduit can be quantifiably reduced by (1) implementing longitudinal ventilation at critical velocity, (2) reducing the exposure surface area, and (3) relocating the installed location from the ceiling to the sidewall.

(5) The proposed performance-based approach can enable the selection of tunnel conduit thermal performance criteria as a function of tunnel geometry, ventilation conditions, conduit configuration, and tunnel traffic composition. Due to the importance of continued operation of a tunnel's electrical systems during an emergency, the thermal performance rating for these conduits can be determined as risk tolerance based on expected fire intensity rather than via simple prescriptive thresholds.

(6) For the conduit considered in this study, performance-based evaluation based on traffic data provided by PennDOT indicated that the following exposure thresholds could be used to develop risk-based fire resistance ratings for conduits that run along the circular tunnel's top-of-ceiling and are fully exposed to fire:

- To withstand a 50-yr return period fire, the conduit and its contents should remain functional after 2 hrs of exposure to 1095°C (consistent with the mean prescribed value in ASTM

E1529) if the tunnel has longitudinal ventilation at critical velocity. Similarly, an exposure temperature of 1500°C would apply for natural ventilation conditions.

- For a 20-yr return period fire, the corresponding temperature demands decrease to 1150°C and 900°C for the natural and longitudinally ventilated cases, respectively.

(7) The MATLAB-SAFIR method is efficient to model the behavior of the concrete liner protected with passive fire protection subjected to fire hazards. Considering the uncertainties associated with the thermal parameters of both concrete liner and protection materials with MCS, the damage maps are developed to help efficiently characterize the damage state of the protected concrete liner.

(8) With the computational efficiency of the confined discretized solid flame (CDSF) model and damage maps developed in this study, the entire tunnel damage along with the repairing time and cost afterward, can be assessed as subjected to specific tunnel fire hazard.

(9) The lifecycle investment for a specific fire protection plan is calculated, containing the installation and maintenance fee, while the lifecycle loss due to the tunnel fire hazard is assessed based on the tunnel traffic and its importance. The uncertainties associated are considered via MCS taking the 95% confidence interval.

(10) The multi-objective optimization via GAs provides optimal solutions while contradictory objectives are applied. This optimization method is flexible in choosing the objectives and constraints as needed according to specific engineering requirements. Carefully choosing the appropriate objective sets can help narrow down decision-making choices.

(11) The factors influencing the optimal solutions include the tunnel traffic and the detour length. Generally, tunnel of smaller size, higher traffic volume, higher HGV percentage, longer detour length requires more protection. The longitudinal ventilation, though required for life safety concerns, is not efficient for mitigating the tunnel structural damage compared to the FFFS and protection boards.

1.2 How have the results been disseminated?

- The results were presented at *Engineering Mechanics Institute Conference*. John Hopkins University*, Baltimore, 2022*

2. Participants and Collaborating Organizations

Name: Lehigh University

Location: Bethlehem, PA

Contribution: (1) Application of the CDSF model; (2) tunnel conduit thermal impact envelop in terms of peak heat flux and exposure time; (3) efficient electrical conduit temperature evaluation method based on finite element thermal analysis; (4) tunnel electrical conduit testing criteria development based on tunnel dimension and traffic; (5) develop the tunnel liner damage assessment method according to thermal impact;

(6) propose tunnel structural fire mitigation plan as a combination of active and passive methods; (7) come up with optimization method for tunnel fire mitigation by accounting the tunnel dimension, tunnel traffic, the investment, and corresponding economic loss; (8) the functionality loss of tunnel subjected to fire hazard is quantified by assessing the repair time.

3. Outputs

Journal publications

- Zhu, Z., Guo, Q., Quiel, S. E., & Naito, C. J., (In press on *Tunnelling and Underground Space Technology*). Performance-Based Evaluation of Exposed Electrical Conduit for Severe Fires in Roadway Tunnels
- Zhu, Z**.**, Quiel, S. E., & Naito, C. J., (under review). Performance-based optimization of structural fire mitigation strategies for roadway tunnels.

Presentations

- Zhu, Z., and Quiel, S. E., "Performance-based optimization of structural fire mitigation strategies for roadway tunnels" at *Engineering Mechanics Institute Conference*. John Hopkins University*, Baltimore, 2022*

4. Outcomes

- Focuses on the fire resistance of steel electrical conduit, which directly affects the functionality of the lighting, ventilation, and other electrical tunnel systems during a fire event. Thermal demand envelopes are developed for typical conduit pipes based on the magnitude of the fire and the exposure of the conduit pipe at several locations in a prototype circular tunnel cross-section. Multiple sensitivity analyses were conducted to examine uncertainties associated with conduit properties, tunnel geometry, and the fire hazard as a function of tunnel traffic.
- A decision-making methodology to optimize the fire mitigation method for roadway tunnels by both minimizing the lifecycle financial cost including the investment and economic loss while maximizing the protection efficiency. The optimization accounts for the performance of the tunnel structure subjected to fire hazard, the post-fire repair procedure, the tunnel traffic, and its importance. These variables are used to develop optimal active and passive fire protection method for the structure studied.

5. Impacts

- Provide a framework to optimize the tunnel fire mitigation plan by considering characteristics of specific plan (i.e., tunnel dimension, tunnel traffic, investment, and loss). The objectives could be changed flexibly as needed. It provides a basis for decision-making.
- The framework of coming up with the testing criteria for tunnel electric conduit could be extend to other non-structural components.